The Meteoritical Society

Meteoritics & Planetary Science 1–22 (2018)
doi: 10.1111/maps.13218

Petrogenesis of lunar impact melt rock meteorite Oued Awlitis 001

Axel WITTMANN[1*], Randy L. KOROTEV[2], Bradley L. JOLLIFF[2], Kunihiko NISHIIZUMI[3], A. J. Timothy JULL[4], Marc W. CAFFEE[5,6], Michael ZANETTI[7], and Anthony J. IRVING[8]

[1]Eyring Materials Center, Arizona State University, 901 S. Palm Walk, PSA 213, Tempe, Arizona 85287–1704, USA
[2]Department of Earth and Planetary Sciences and the McDonnell Center for the Space Sciences, Washington University in St. Louis, One Brookings Drive, St. Louis, Missouri 63130, USA
[3]Space Sciences Laboratory, University of California Berkeley, Berkeley, California 94720–7450, USA
[4]Department of Geosciences, University of Arizona, 1040 East Fourth St., Tucson, Arizona 85721–0077, USA
[5]Department of Physics and Astronomy, Purdue University, 525 Northwestern Avenue, West Lafayette, Indiana 47907–2036, USA
[6]Department of Earth, Atmospheric, and Planetary Sciences, Purdue University, 525 Northwestern Avenue, West Lafayette, Indiana 47907–2036, USA
[7]Department of Earth Sciences, University of Western Ontario, 1151 Richmond Street N, London, Ontario N6A 5B7, Canada
[8]Department of Earth and Space Sciences, University of Washington, 4000 15th Avenue NE, Seattle, Washington 98195, USA
*Corresponding author. E-mail: axel.wittmann@asu.edu

(Received 15 March 2018; revision accepted 17 October 2018)

Abstract–Oued Awlitis 001 is a highly feldspathic, moderately equilibrated, clast-rich, poikilitic impact melt rock lunar meteorite that was recovered in 2014. Its poikilitic texture formed due to moderately slow cooling, which judging from textures of rocks in melt sheets of terrestrial impact structures, is observed in impact melt volumes at least 100 m thick. Such coherent impact melt volumes occur in lunar craters larger than ~50 km in diameter. The composition of Oued Awlitis 001 points toward a crustal origin distant from incompatible-element-rich regions. Comparison of the bulk composition of Oued Awlitis 001 with Lunar Prospector 5° γ-ray spectrometer data indicates a limited region of matches on the lunar farside. After its initial formation in an impact crater larger than ~50 km in diameter, Oued Awlitis 001 was excavated from a depth greater than ~50 m. The cosmogenic nuclide inventory of Oued Awlitis 001 records ejection from the Moon 0.3 Ma ago from a depth of at least 4 m and little mass loss due to ablation during its passage through Earth's atmosphere. The terrestrial residence time must have been very short, probably less than a few hundred years; its exact determination was precluded by a high concentration of solar cosmic ray-produced ^{14}C. If the impact that excavated Oued Awlitis 001 also launched it, this event likely produced an impact crater >10 km in diameter. Using petrologic constraints and Lunar Reconnaissance Orbiter Camera and Diviner data, we test Giordano Bruno and Pierazzo as possible launch craters for Oued Awlitis 001.

INTRODUCTION

Oued Awlitis 001 (OA 001) is a 7.7 × 6.6 × 3.5 cm brownish-gray lunar meteorite with a preserved, translucent fusion crust that was found as two fitting pieces in 2014 in Morocco/Western Sahara (Irving and Aid in Ruzicka et al. 2017; Wittmann et al. 2014a, 2015; Nishiizumi et al. 2016; Ferrière et al. 2017). The main 382 g piece (Fig. 1A) was excavated from shallow depth during a search for firewood; the 50.5 g piece was recovered a month later near the same location and preliminary data (Ferrière et al. 2017) confirms its petrology is consistent with material from the main mass of OA 001 (Wittmann et al. 2014a, 2015).

The mineralogy and whole-rock chemistry establish this specimen as a lunar meteorite as described by Wittmann, Irving, Carpenter, Korotev, and Kuehner in the Meteoritical Bulletin (Ruzicka et al. 2017). Our

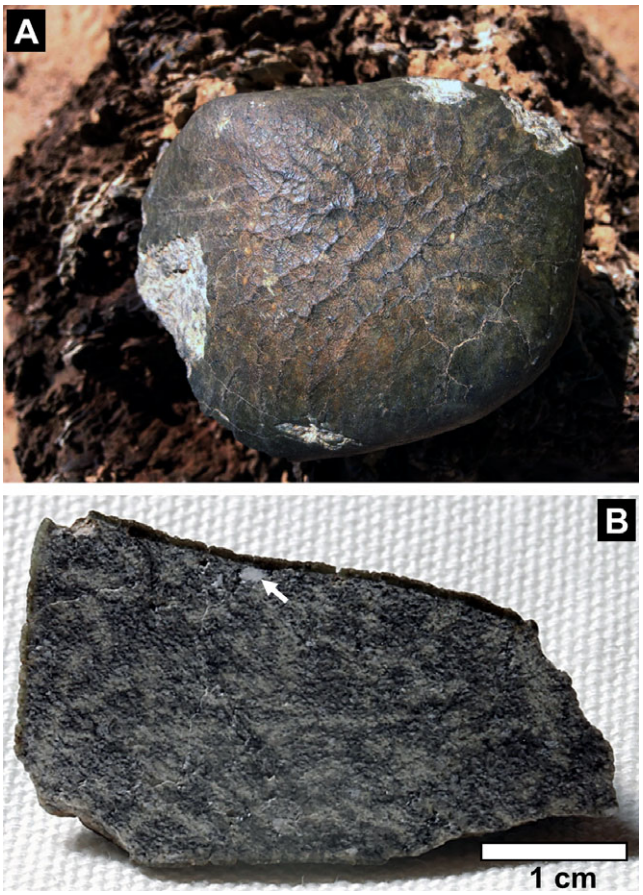

Fig. 1. Lunar meteorite Oued Awlitis 001. A) Main mass at its find location. The maximum dimension of the stone is 7.7 cm. Photo courtesy of M. Aid. B) Photograph of the cut face of our sample specimen. Note thin fusion crust on top and left side and single, ca. 2 mm long, rounded white clast (arrow).

initial petrographic and chemical analyses of OA 001 indicated that it is a rare poikilitic melt rock lithology, tempting us to further investigate its origin.

Provenance studies for lunar meteorites are performed routinely based on the comparison of chemical data from small chips of lunar rocks to the composition of large regions on the Moon as determined by the Lunar Prospector γ-ray spectrometer (e.g., Jolliff et al. 2000, 2014; Korotev et al. 2003; Korotev 2005; Joy et al. 2010, 2011, 2014; Mercer et al. 2013; Wittmann et al. 2014b; Calzada-Diaz et al. 2015, 2016). Our study aims to refine this approach for the identification of potential source craters for OA 001 by including the analysis of high-resolution Lunar Reconnaissance Orbiter Camera (LROC) images and Diviner nighttime temperature distribution and rock abundance maps (Robinson et al. 2010; Hayne et al. 2017). LROC and Diviner have yielded a wealth of detailed data for the surface of the Moon. Among other scientific objectives, these data allowed refining model ages for surface features on the Moon (e.g., Hiesinger et al. 2012; Kirchoff et al. 2013; Kramer et al. 2013; Braden et al. 2014; Ashley et al. 2016; Krüger et al. 2016; Shirley et al. 2016; Clark et al. 2017; Orgel et al. 2018; Van der Bogert et al. 2017; Zanetti et al. 2017; Povilaitis et al. 2018), unraveling lithologic variations associated with impact craters (Bray et al. 2010, 2018; Spudis et al. 2011; Ashley et al. 2012; Denevi et al. 2012; Plescia and Cintala 2012; Plescia and Spudis 2014; Stopar et al. 2014; Wagner and Robinson 2014; Meyer et al. 2016; Robinson et al. 2016; Spudis and Sliz 2017), and revealing young impact craters based on characteristics of the albedo and surface roughness associated with their ejecta (Bandfield et al. 2011; Cahill et al. 2014; Ghent et al. 2014, 2016; Greenhagen et al. 2016; Williams et al. 2016; Hayne et al. 2017). However, linking LROC and Diviner data to lunar meteorites has not been attempted so far. If successful, remote sensing data from the Moon could be related to the composition and nature of lunar rocks, and age models would be anchored to absolute ages of lunar meteorites. The full potential of lunar samples from random regions on the Moon—348 recognized stones of an estimated 138 meteorites with a combined weight of 275 kg (as of September 25, 2018, according to the Meteoritical Bulletin and coauthor Korotev's compilation of lunar meteorite data at http://meteorites.wustl.edu/lunar/moon_meteorites_list_alumina.htm)—could be realized for the exploration of lunar geology and the impact cratering of the inner solar system.

Thus, using its petrography, bulk rock and mineral chemistry, and its cosmogenic nuclide inventory, we explore the petrogenesis of OA 001. By comparing our reconstruction of the petrogenesis of OA 001 with Lunar Prospector and Lunar Reconnaissance Orbiter remote sensing data, we then constrain its provenance on the Moon.

SAMPLES AND METHODS

Our sample (Fig. 1B) is a ~4 × 2 cm wide rock with a partly preserved fusion crust from the main mass of OA 001. The sample specimen has a homogenous texture with only one conspicuous, approximately 2 × 1 mm grayish-white, rounded clast. We estimated the modal abundance of clast components using the National Institute of Health's ImageJ (imagej.nih.gov/ij/) image analysis software on a scan image of our 380 mm^2 thin section of OA 001. We cropped the margins of our image prior to these analyses to exclude the regions of our thin section with fusion crust. By setting appropriate thresholds for the scanned image

that effectively separated the relatively more bright plagioclase mineral clasts from the groundmass and phenocryst plagioclase, we determined the modal proportion of plagioclase clasts in repeated measurements. Moreover, we analyzed this thin section under the optical microscope and determined the compositions of mineral and melt components by electron microprobe analysis (EMPA). Major, minor, and trace element concentrations of eight 25–32 mg subsamples were determined by instrumental neutron activation analysis (INAA) coupled with EMPA on fused beads of powdered INAA sample material (Korotev et al. 2009; Korotev 2012, 2017). Cosmic ray exposure ages and a terrestrial residence age were derived from the measurement of cosmogenic nuclides on a 3 mm thick, 304 mg sample of OA 001 that contained fusion crust.

Electron Microprobe Analysis

We obtained chemical compositions from the thin section of OA 001 using a JEOL JXA-8200 electron microprobe at the Department of Earth and Planetary Sciences of Washington University in Saint Louis and the JEOL JXA-8530F electron microprobe at the Eyring Materials Center of Arizona State University. For olivine, pyroxene, and FeNi metal analysis, we used an accelerating voltage of 15 kV, a beam current of 15 nA, and a beam diameter of ~1 μm; we defocused the beam diameter to 5 and 10 μm for analyses of plagioclase, fusion crust, and glassy shock melt. Concentrations of the elements Si, Ti, Al, Fe, Ca, Mg, Na, K, Cr, P, S, and Mn in silicates and oxides were analyzed by wavelength-dispersive spectrometry using count times of 10–20 s on peaks and background positions. The data were processed using the Probe for EPMA software by Probe Software, Inc. Calibration and data reduction was done with measurements on well-characterized natural and synthetic standard materials and yielded typical detection limits for the analyses in St. Louis of 0.03 wt% for MgO, Al_2O_3, and K_2O; 0.04 wt% for Na_2O, TiO_2, and Cr_2O_3; 0.05 wt% for SiO_2; 0.06 wt% for P_2O_5 and SO_3; 0.07 wt% for CaO and NiO; and 0.08 wt% for MnO and FeO; using longer counting times of 30–10 s on peaks and background positions, the analytical sessions in Tempe yielded the following detection limits for an otherwise similar analytical setup: 0.02 wt% for MgO, Al_2O_3, CaO, Na_2O, and K_2O; 0.03 wt% for TiO_2, SiO_2 and Cr_2O_3; 0.06 wt% for MnO and FeO.

We acquired intensity maps for the kα-X-ray lines of Al, Si, Ca, Mg, and Fe for selected regions on the thin section of OA 001 by using a focused beam with a 15 kV accelerating voltage, a beam current of 24 nA, and a dwell time of 10 ms with the Jeol JXA-8530F.

Instrumental Neutron Activation Analysis and Fused Bead EMPA

Following methods we have previously used for lunar meteorites (Korotev et al. 2009; Korotev 2012, 2017), we analyzed eight 25–32 mg subsamples of the main mass of OA 001 by INAA. After INAA, we pulverized two of these INAA subsamples in an agate mortar and fused the powders to glass beads using a molybdenum strip resistance heater under an Ar atmosphere (Jolliff et al. 1991; Zeigler et al. 2005). We prepared a polished mount of the fused glass beads and analyzed them with the JEOL JXA-8200 electron microprobe in the Department of Earth and Planetary Sciences at Washington University in Saint Louis. For these analyses, we made 10 spot measurements on each of the fused beads, using beam diameters of 20 μm, an accelerating voltage of 15 kV, and a beam current of 25 nA to determine the concentrations of the elements Si, Ti, Al, Cr, Fe, Mn, Mg, Ca, Na, K, P, S, and Mo. Detection limits for these analyses were 0.02 wt% for MgO, Al_2O3, K_2O, and SO_3; 0.03 wt% for CaO, Na_2O, and P_2O_5; 0.04 wt% for SiO_2, TiO_2, and MoO_3; 0.06 wt% for MnO and FeO; and 0.07 wt% for Cr_2O_3. Assuming all MoO_3 was incorporated into the glass beads from the Mo-metal strips, we recalculated the oxide abundances to MoO_3-free concentrations.

Cosmogenic Nuclides

Our 3 mm thick, 304 mg sample for cosmogenic nuclide studies had exposed fusion crust. We split the sample to two portions, a 203 mg split that includes fusion crust for ^{10}Be (half-life 1.36 Ma; Nishiizumi et al. 2007), ^{26}Al (half-life 0.705 Ma; Norris et al. 1983), and ^{36}Cl (half-life 0.30 Ma) measurements and a 101 mg split for ^{14}C (half-life 5,740 a) measurement (Nishiizumi 2004).

^{10}Be, ^{26}Al, and ^{36}Cl Measurements

To eliminate weathering products, we etched the portion of OA 001 that included fusion crust twice with a 0.2 N HNO_3 solution in an ultrasonic bath for 10 min, resulting in a 5.3% weight loss. After grinding and weighing, we dissolved the clean sample in an HF-HNO_3 mixture along with Be and Cl carriers. We then did a routine chemical assay to determine the concentration of elements relevant to the calculation for production rates of cosmogenic nuclides. For these measurements, we used ICP-OES. Because small samples tend to be chemically inhomogeneous, we measured target elemental compositions in an aliquot of the sample we used for the cosmogenic radionuclide measurements. After these measurements, we added Al and Mn carriers, and chemically separated and purified Be, Al, Cl, and Mn for accelerator mass spectrometry

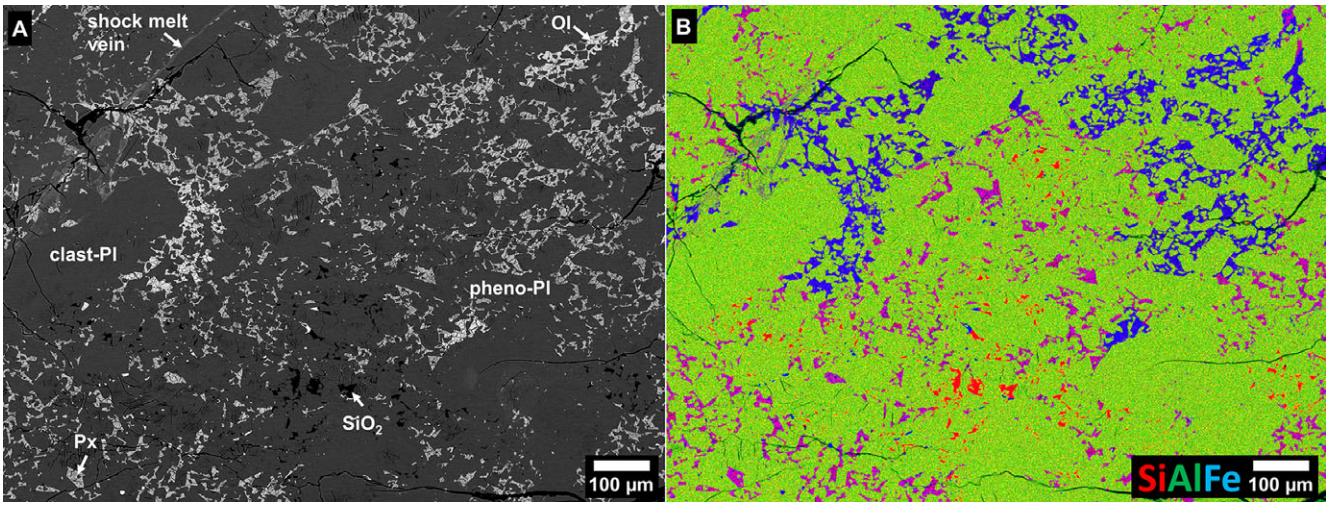

Fig. 2. Texture of Oued Awlitis 001. A) Backscattered electron (BSE) image illustrating textural relationships in Oued Awlitis 001. Ol is olivine, Px is pyroxene, Pl is plagioclase, "pheno-Pl" means phenocryst plagioclase. B) Combined X-ray intensity maps of silicon, aluminum, and iron from the same region as in A.

(AMS) measurements (e.g., Nishiizumi et al. 1984a, 1984b). We performed the ^{10}Be, ^{26}Al, and ^{36}Cl AMS measurements at PRIME Lab (Sharma et al. 2000). After correcting for the ^{10}Be background due to the chemical blank, we normalized the measured ratios to ICN ^{10}Be, NBS ^{26}Al, and NBS ^{36}Cl AMS standards (Sharma et al. 1990; Nishiizumi 2004; Nishiizumi et al. 2007). In addition to repeated measurements of the primary standards used for normalization, we measured secondary standards of differing ratios throughout the run. We normalized all ICP-OES measurements using calibrated ICP standards. The uncertainties (1σ) in the activities of the ^{10}Be, ^{26}Al, and ^{36}Cl are dominated by the analytical uncertainties of the AMS measurement.

Terrestrial Residence Age

To measure ^{14}C, we first pretreated a ~110 mg sample of OA 001 with 85% H_3PO_4 to remove weathering products. We then washed and dried the residue (97 mg) and melted it with a Fe flux in the presence of oxygen in a radio-frequency furnace. The released gases were purified and isolated in a gas-flow system. We converted the captured $^{14}CO_2$ to graphite and measured the ^{14}C by AMS at the University of Arizona AMS facility (Donahue et al. 1990a, 1990b; Jull et al. 1998).

RESULTS

Petrography

Macroscopic Observations

The single stone has a yellow-brownish-translucent fusion crust that displays a dark vein network as dendritic ridges on the surface (Fig. 1A). Small, yellow-white components are visible through the fusion crust. On chipped parts, the rock is whitish-gray. A cut sample surface is fine-grained and consists of a gray groundmass that is intergrown with anhedral domains of grayish-white minerals (Fig. 1B).

Petrography and Mineral and Melt Chemistry

Under a microscope, OA 001 displays a poikilitic texture of intensely fractured, mm-sized olivine ($Fo_{55.8–71.0}$, $n = 24$) and pyroxene ($En_{42.2–59.4}Fs_{19.6–41.7}Wo_{6.4–34.0}$; $n = 27$) crystals that enclose euhedral plagioclase phenocrysts ($An_{94.3–97.3}Ab_{2.6–5.5}Or_{0.0–0.2}$; $n = 25$) that are typically <100 μm (Fig. 2; Tables S1–S3 in supporting information). The olivine and pyroxene oikocrysts are compositionally zoned; olivine exhibits Mg-rich cores and Fe-rich rims, while pyroxene displays pigeonite rims and augite cores. This crystallized melt groundmass also envelops partly assimilated, <1 mm, angular to subhedral plagioclase clasts ($An_{88.1–97.9}Ab_{2.1–11.6}Or_{0.0–0.3}$; $n = 27$) that account for approximately 20 vol% plagioclase mineral clasts of our thin section. These plagioclase clasts are distinguished by irregular and subplanar fractures and a larger compositional variation compared to the smaller plagioclase phenocrysts. In cross-polarized light, plagioclase clasts and phenocrysts show reduced birefringence, exhibit strongly undulating extinction, and are partly isotropic. Some plagioclase grains exhibit mechanical twinning. Commonly, plagioclase in OA 001 displays faint planar deformation features mostly in one direction and occasionally in two directions (Fig. 3). The intense shock metamorphic overprint obscures compositional zoning in plagioclase.

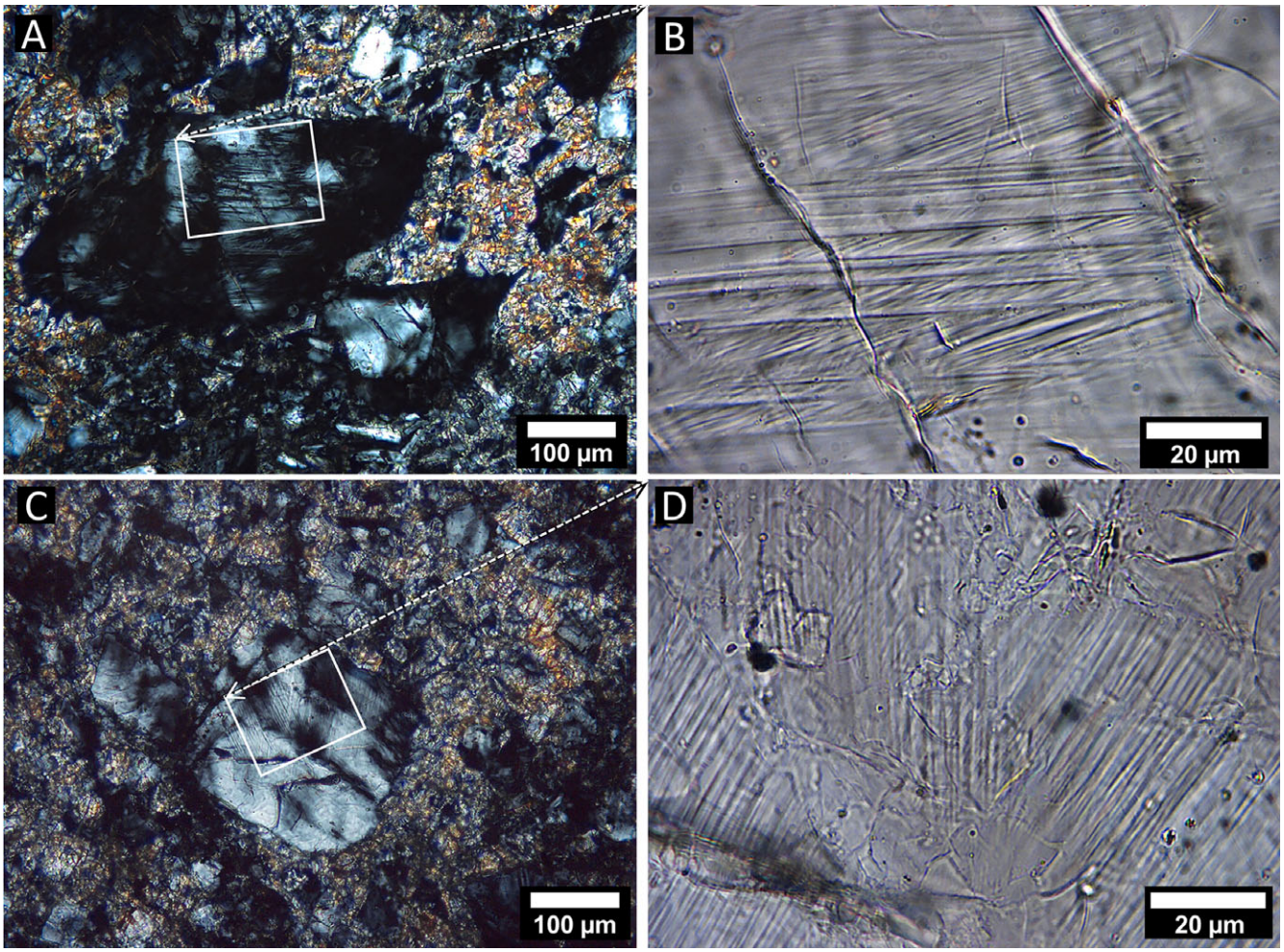

Fig. 3. Shock metamorphic features in Oued Awlitis 001 plagioclase. A and C) Partly isotropic plagioclase clasts with strongly undulating extinction, cross-polarized light. B and D) Cores of plagioclase clasts exhibit two sets of planar deformation features, plane polarized light.

In places, up to ~20 μm SiO_2 fills interstitial space between densely packed plagioclase phenocrysts (Fig. 2).

Plagioclase clasts and the poikilitic groundmass contain euhedral, up to 10 μm FeNi metal grains and up to 70 μm troilite grains (Table S4 in supporting information). Ilmenite and Ti-rich spinel (Table S5 in supporting information) are <10 μm accessory phases that are intergrown in some cases and may contain <<1 μm domains of FeNi metal.

Small, <100 μm brown and black shock melt pockets occur as pods (Figs. 4A–C), or as <10 μm thick, continuous veinlets that offset the crystal fabric (Figs. 2 and 4A). Their compositions vary depending on the host mineralogy (Table S6 in supporting information).

Vesicular fusion crusts up to 150 and 500 μm thick occur on two opposite sides of the thin section (Fig. 5). The thicker fusion crust displays whisker crystals. Heating affected the side of the thicker fusion crust to a depth of ~300 μm, where the olivine and pyroxene oikocrysts have been melted (Fig. 5). The composition of the outer, glassy fusion crust is close to the bulk rock composition of OA 001. In contrast, the composition of the partly remelted internal portion of the fusion crust reflects selective melting of pyroxene and olivine (Table S6).

Based on the optical properties of plagioclase in OA 001, the occurrence of planar deformation features and its partial transformation to diaplectic glass, an equilibrium shock metamorphic overprint of 20–24 GPa is indicated (Fritz et al. 2011, 2017; Stöffler et al. 2018). Shock melt veins and pockets are disequilibrium shock features that likely formed due to the closing of vesicles or pore and fracture space during the passage of a shock wave.

Other than a ~10 μm wide, irregular fracture that is filled with brown clay minerals, no secondary terrestrial alteration is apparent in our thin section.

Bulk Rock Chemistry

The bulk rock chemistry of OA 001 (Table 1; Fig. 6) indicates the normative composition of a noritic anorthosite that is similar to ferroan anorthositic rocks from the Apollo collection (e.g., Stöffler et al. 1980). Its magnesium number (mol% Mg/[Mg+Fe] = 56.6) is one of the lowest among the currently known feldspathic meteorites (Fig. 6), whereas its chemical composition is typical for feldspathic lunar meteorites (Korotev 2012, 2017). The CI chondrite-normalized (CN) rare earth element (REE) pattern of OA 001 (Fig. 7) is relatively flat (La/Yb = 1.9) and indicates a 3.5–6.6× enrichment relative to CI chondrites (Anders and Grevesse 1989). We interpolated the concentrations of Gd using the concentrations of Ce, Sm, Tb, and Yb that were determined by INAA to calculate a moderately positive Eu-anomaly ($Eu/Eu^* = [(Eu_{CN})/([Sm_{CN} \times Gd_{CN}]^{0.5})]$) of 3.1 in OA 001 using the CN concentrations of Eu, Gd, and Sm.

Target Element Compositions and Concentrations of Cosmogenic Nuclides of OA 001

Concentrations of cosmogenic radionuclides and target elements of OA 001 are shown in Table 2. The concentrations and nuclide ratios of ^{10}Be and ^{36}Cl in OA 001 indicate that the observed radionuclides (Table 2) were produced by 4π irradiation in space during transit from the Moon to Earth. The high ^{14}C activity in OA 001 indicates solar cosmic ray (SCR) production (Jull et al. 1998). The excess ^{14}C in OA 001 is 42 ± 14 dpm/kg, assuming a 4π galactic cosmic ray (GCR) production rate of 65 atom ^{14}C/min/kg. We could not calculate terrestrial ages for OA 001 because of the high concentration of SCR-produced ^{14}C. There is no significant decay of ^{14}C, indicating that the meteorite has a short terrestrial age, probably less than a few hundred years.

DISCUSSION

Lunar Origin

The mineral (Fig. 8 A–B; Tables S1–S5) and bulk rock chemistry (Table 1) of OA 001 is typical for feldspathic lunar rocks in the meteorite, Apollo, and Luna collections (cf. Papike 1998; http://meteorites.wustl.edu/lunar/; last accessed February 9, 2018).

Implications from Cosmogenic Nuclides in OA 001

We determined exposure age and ejection depth of OA 001 using techniques described in previous studies (cf. Nishiizumi et al. 1991). If the excess ^{14}C of 42 ± 14 dpm/kg in OA 001 was produced by SCR, the production must have occurred at a depth of <1 g cm^{-2}

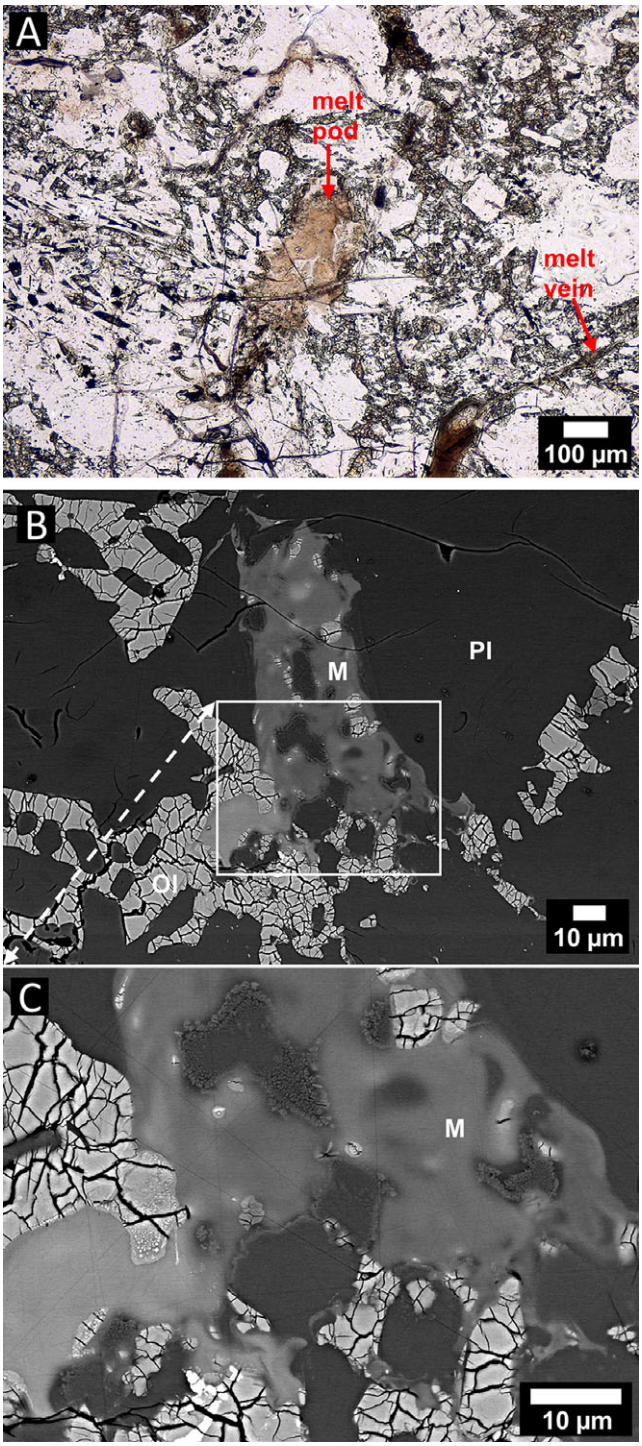

Fig. 4. Shock melt veins and pockets in Oued Awlitis 001. A) Brown to black shock melt veins and shock melt pockets crosscut the poikilitic texture, linear polarized light micrograph. B and C) Shock melt pocket (M) that formed in plagioclase (Pl) and olivine (Ol); backscattered electron images.

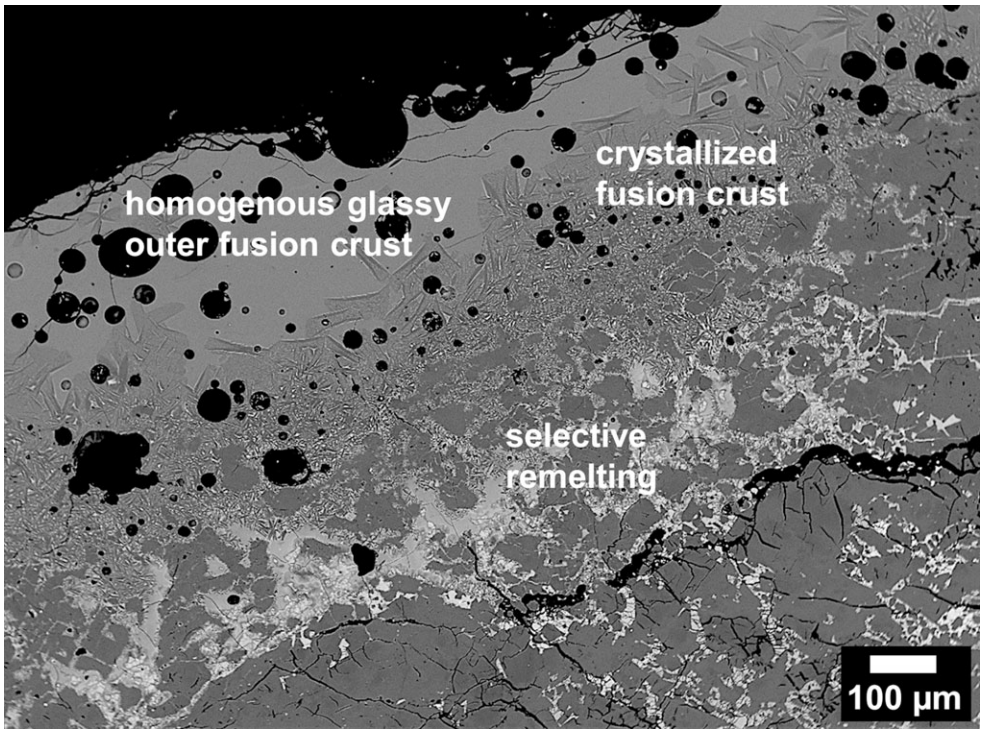

Fig. 5. Oued Awlitis 001 fusion crust. Thick, partly preserved fusion crust illustrates the effects and depth of melting during Oued Awlitis 001's passage through Earth's atmosphere; Pl = plagioclase; Px = pyroxene; Ol = olivine; BSE image.

in the pre-atmospheric body of OA 001 and the ablation depth must be <3 mm. The existence of a large amount of SCR-produced ^{14}C suggests that the size of the recovered meteorite is nearly the same as its pre-atmospheric size, independent of whether it was a 2π or a 4π exposure. We calculate a 4π production rate of ^{10}Be near the surface of OA 001 of ~18 atom/min/kg based on the chemical composition of OA 001 and a radius of 3–4 cm (Table 2) (e.g., Masarik and Reedy 1994). The ^{10}Be-^{36}Cl 4π exposure age, that is to say the transit time from the Moon to Earth, of OA 001 is 0.30 ± 0.02 Ma (cf. Herzog and Caffee [2014] for a summary of CRE calculations). Using this exposure age, we calculate that the saturation value of ^{26}Al in OA 001 is 343 ± 20 dpm/kg. After accounting for the GCR production near the surface of ~65 atom/min/kg and a radius of 3–4 cm, we find that OA 001 has an ^{26}Al excess of ~280 dpm/kg, which must have been produced by SCR at a depth of ~1 g cm^{-2} (Nishiizumi et al. 2009). The pre-atmospheric depth we infer from SCR-produced ^{26}Al is in good agreement with our ablation estimation using SCR-produced ^{14}C. While many lunar meteorites exhibit SCR effects, OA 001 and Calcalong Creek (Nishiizumi et al. 1992) contain the highest known concentrations of SCR-produced nuclides among lunar meteorites.

The ejection depth of OA 001 is >800 g cm^{-2} on the Moon. This depth would mean that OA 001 was completely shielded from cosmic ray exposure before ejection, i.e., its depth of excavation must have been at least ~4 m.

Lunar Poikilitic Rocks

Poikilitic rocks are characterized by their texture of large, optically continuous crystals (oikocrysts) of one mineral type that encloses many smaller crystals (chadacrysts) of other mineral phases. Many poikilitic impact melt rocks have been identified in the Apollo collections (e.g., Vaniman and Papike 1980; Spudis and Ryder 1981; Papike et al. 1998). Simonds et al. (1973) noted that poikilitic rocks have been found at all non-mare landing sites on the Moon and that "virtually all" poikilitic Apollo rocks have "low-K-KREEP composition." Poikilitic rocks are common lithologies on the Moon, for example, poikilitic rock fragments constitute about 10% of the 2–4 mm grain-size fractions of soils from all Apollo 16 sampling localities except Station 11 (Delano et al. 1973).

Simonds et al. (1973) and Simonds (1975) suggested that poikilitic textures stem from two-stage cooling of impact melts; during disequilibrium at higher cooling rates, small feldspar phenocrysts would form rapidly before equilibrium crystallization at lower cooling rates would produce pyroxene and olivine oikocrysts.

Table 1. Bulk rock composition of lunar meteorite OA 001.

	Fused bead EMPA			Instrumental neutron activation analysis				
	Average of 20 spot analyses		1σ	Meteorite stone and subsample		Mass-weighted mean	Sampling uncertainty	Analytical uncertainty
SiO_2	wt%	44.4	0.24	Na_2O	wt%	0.361	0.008	0.007
TiO_2	wt%	0.19	0.03	CaO	wt%	17.2	0.4	0.4
Al_2O_3	wt%	30.9	0.43	Sc	ppm	6.41	0.34	0.13
Cr_2O_3	wt%	0.11	0.03	Cr	ppm	408	8	8
FeO[a]	wt%	3.47	0.22	FeO	wt%	3.45	0.21	0.07
MnO	wt%	0.07	0.03	Co	ppm	8.49	0.37	0.17
MgO	wt%	2.54	0.14	Ni	ppm	51	6	8
CaO	wt%	17.6	0.11	Zn	ppm	3	1	1
Na_2O	wt%	0.36	0.03	As	ppm	0.15	0.09	0.16
K_2O	wt%	0.03	0.01	Br	ppm	0.07	0.02	0.08
P_2O_5	wt%	0.02	0.03	Rb	ppm	0.7	0.3	0.4
SO_3	wt%	0.04	0.02	Sr	ppm	168	5	8
Total	wt%	99.8	0.23	Zr	ppm	20	5	7
Mg#	mol%	56.6	n.a.	Sb	ppm	0.03	0.06	0.03
Pl[b]	vol%	89.0	n.a.	Cs	ppm	0.010	0.004	0.013
Opx[b]	vol%	5.4	n.a.	Ba	ppm	23	2	3
Cpx[b]	vol%	3.5	n.a.	La	ppm	1.55	0.10	0.03
Ol[b]	vol%	2.2	n.a.	Ce	ppm	3.92	0.30	0.09
				Nd	ppm	2.9	0.3	0.6
				Sm	ppm	0.746	0.051	0.015
				Eu	ppm	0.824	0.015	0.017
				Tb	ppm	0.157	0.009	0.006
				Yb	ppm	0.599	0.035	0.016
				Lu	ppm	0.085	0.005	0.002
				Hf	ppm	0.527	0.024	0.015
				Ta	ppm	0.102	0.025	0.010
				Ir	ppb	2.3	0.2	0.4
				Au	ppb	1.4	0.4	0.5
				Th	ppm	0.214	0.009	0.008
				U	ppm	0.08	0.02	0.03
				mass	mg	236.49	n.a.	n.a.

EMPA = electron microprobe analysis; σ = standard deviation; Sampling uncertainty = 95% confidence limits based on $N = 8$ subsamples; Analytical uncertainty = 2-standard deviation estimate of analytical uncertainty of a single subsample based mainly on counting statistics; n.a. = not applicable. Mg# is molar Mg/(Mg+Fe).

[a]All Fe as FeO.

[b]Calculated CIPW-normative mineralogy, normalized to 100 vol% (e.g., Rollinson 1993).

Furthermore, Simonds et al. (1973) noted that the poikilitic rocks from the Apollo landing sites typically contain cavities that are interpreted as degassing vesicles. Lofgren (1977) showed with melting experiments that poikilitic textures can result from high-density nucleation sites in impact melts charged with μm to sub-μm crystal clasts; previously, this was inferred by Ryder and Bower (1976) for incompatible-element-rich Apollo 14 poikilitic impact melt rocks.

Its composition (Fig. 6) that includes a small relative enrichment in highly siderophile elements, e.g., 2.3 ± 0.2 ppb Ir (Table 1), and fine-grained poikilitic, clast-rich texture, suggest that OA 001 does not represent a pristine, endogenous lunar lithology (Warren 1993). Instead, OA 001 offers a fresh perspective on the generation of poikilitic impact melts on the Moon because its very low incompatible element contents and aluminous bulk composition (Table 1; Fig. 7) indicate a formation from highly feldspathic target rocks, far away from the Apollo landing sites that were within or nearby incompatible-element-rich rocks of the Procellarum KREEP terrane (Jolliff et al. 2000).

Comparison With Poikilitic Rocks Similar to OA 001

Poikilitic textures such as the one observed in OA 001 are known to occur in impact melt rocks that crystallize from melt volumes on the order of 100 m

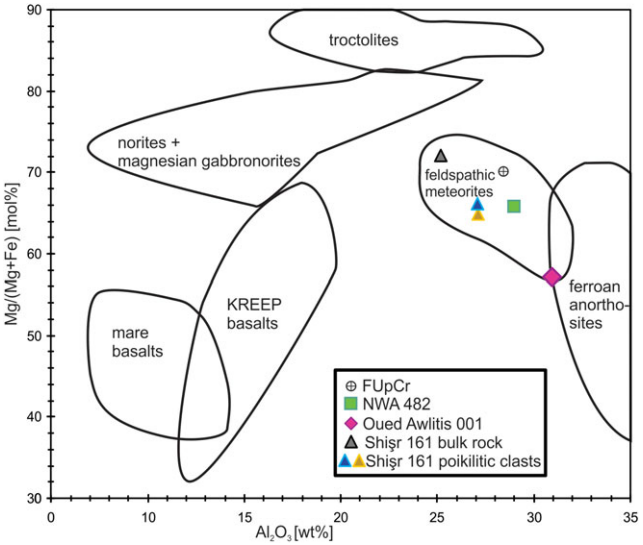

Fig. 6. Reconstructed bulk compositions of lunar rocks in Al_2O_3 versus Mg/(Mg+Fe) space. Diagram modified after Wittmann et al. (2014b); bulk compositions of Shişr 161 after Korotev (2012), bulk composition of Northwest Africa (NWA) 482 and the FUpCr (feldspathic upper crust) after Korotev et al. (2003); poikilitic clasts in Shişr 161 after Wittmann et al. (2014b).

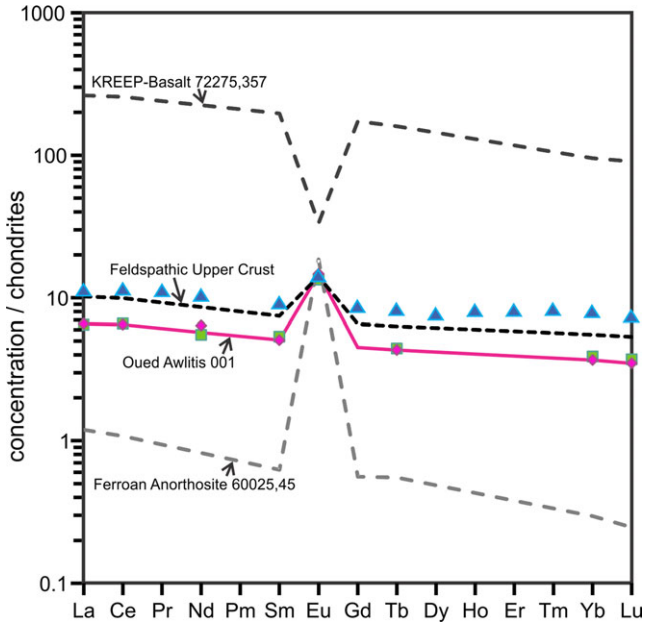

Fig. 7. CI chondrite-normalized rare earth element abundances in Oued Awlitis 001. REE abundances in Oued Awlitis 001 (pink diamonds and pink line) are compared to Apollo KREEP-basalt 72275,375 (Salpas et al. 1987), Apollo ferroan anorthosite 60025,45 (Haskin et al. 1973), lunar meteorite NWA 482 (green squares; Korotev et al. 2003), and a poikilitic impact melt clast in lunar meteorite Shişr 161 (blue triangles; Wittmann et al. 2014b); element concentrations are normalized with CI chondrite data in Anders and Grevesse (1989). Note that the concentrations for Pr, Nd, Pm, Gd, Dy, Ho, Er, and Tm in the INAA data sets have been estimated based on the concentrations of Ce, Sm, Tb, and Yb.

thick; a well-studied example is the "Middle Unit" of the remnant 200–300 m thick impact melt sheet of the ~90 km diameter Manicouagan impact structure in Quebec, Canada. Floran et al. (1978) described this impact melt rock as a fine-grained, clast-bearing impact melt with a poikilitic texture. Another example occurs in the central portion of an ~80 m thick, clast-rich, poikilitic melt rock in the Mistastin Lake impact structure in Labrador, Canada that formed largely from anorthositic target rocks (Grieve 1975; Marion and Sylvester 2010). It is worth noting, though, that this Mistastin Lake poikilitic impact melt rock contains abundant mesostasis glass and, thus, only represents an incipient stage of the formation of a poikilitic texture. In contrast, OA 001 does not retain glassy melt mesostasis (discounting the shock melts that are not related to the poikilitic crystallization), suggesting it cooled much more slowly in a presumably larger volume of impact melt, possibly 100–1000 m thick. Impact melt volumes with a thickness approaching 1000 m tend to differentiate (Wittmann et al. 2014b), which has been observed at >800 m thick impact melt sheets of the Sudbury (Grieve et al. 1991; Therriault et al. 2002), Manicouagan (Spray and Thompson 2008), and Morokweng impact structures (Hart et al. 2002) but is not indicated for OA 001. The relative high uncertainty in our estimated melt thickness related to the formation of poikilitic textures in impact melts on the Moon is meant to account for the possible differences in lunar and terrestrial impact melt crystallization conditions (cf. Cassanelli and Head 2016). For example, Spray et al. (2010) noted that Manicouagan

Table 2. Concentrations of cosmogenic nuclides and target elements in OA 001.

Element or isotope	Concentration	Abundance
Mg	%	1.42
Al	%	16.29
K	ppm	180
Ca	%	12.37
Ti	ppm	1030
Mn	ppm	368
Fe	%	2.43
Co	ppm	10
Ni	ppm	56
^{10}Be	dpm/kg meteorite	2.550 ± 0.019
^{14}C	dpm/kg meteorite	107 ± 14
^{26}Al	dpm/kg meteorite	87.7 ± 1.8
^{36}Cl	dpm/kg meteorite	11.12 ± 0.29
^{36}Cl	dpm/kg (16K+8Ca+Fe)	10.94 ± 0.29

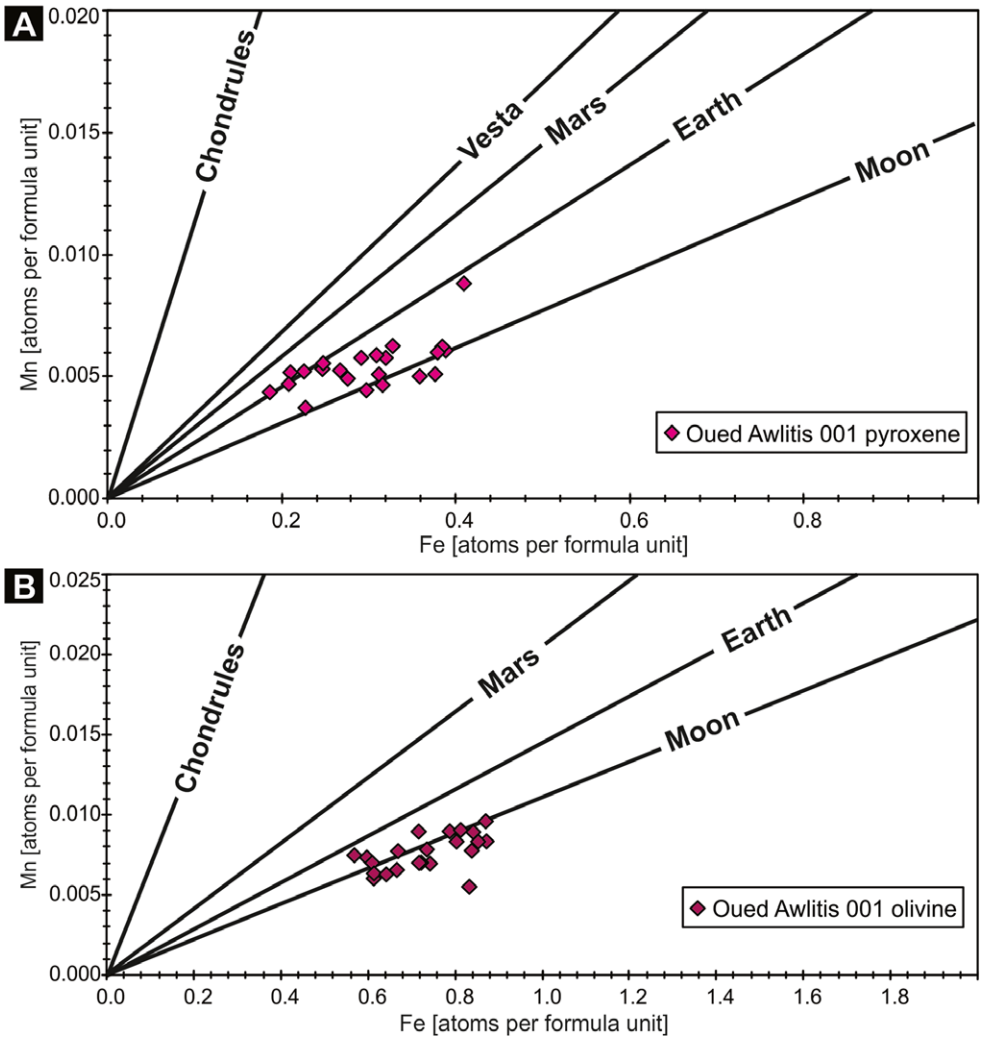

Fig. 8. Molar Fe versus Mn for pyroxene and olivine in planetary melt rocks with approximate trend lines redrawn after Papike (1998).

anorthosite target rocks are dominated by An_{50} plagioclase and Pickersgill et al. (2015) reported similar anorthosite plagioclase compositions of $An_{47–55}$ from Mistastin Lake compared to the $An_{88–98}$ plagioclase in OA 001; interestingly, Pickersgill et al. (2015) did not find PDF in any plagioclase of their Mistastin Lake impactite samples, in contrast to the PDF in OA 001 plagioclase clasts (Fig. 3). On the other hand, equilibration of impact melt sheets with cold debris and subsequent cooling is considered principally similar on the Earth and the Moon based on insulating properties of surrounding rocks and conductive heat loss from the surface (Onorato et al. 1978). The relative higher volatile content in terrestrial target rocks compared to lunar conditions is of minor importance in this context because impact melt boils off volatiles upon decompression from shock loading (Melosh and Artemieva 2004); hence, impact melts are characteristically dry compared to volcanic glass (Beran and Koeberl 1997). While hydration of impact melt may result from the resorption of unmelted debris, impact melt sheets are considered impervious to fluid entrainment until they crystallized and are subject to brittle deformation and infiltration by hydrothermal fluids (Abramov and Kring 2004, 2007).

We are aware of only one other lunar meteorite that displays a texture similar to that in OA 001, namely Northwest Africa (NWA) 482, which is also fresh, has a preserved fusion crust, and a young terrestrial residence age of 8.6 ± 1.3 ka (Daubar et al. 2002; Warren et al. 2005). Moreover, NWA 482 also exhibits glassy shock melt veins, possibly suggesting similar excavation and launch conditions to those for OA 001. However, NWA 482 is chemically distinct (Fig. 6) and displays a polymict clast inventory, which

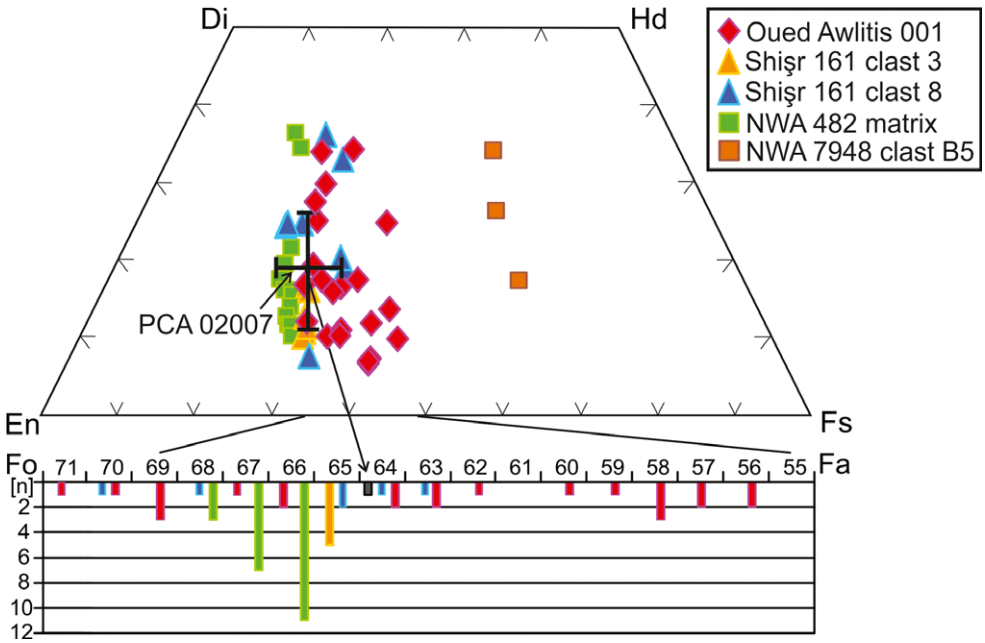

Fig. 9. Pyroxene and olivine compositions in lunar poikilitic impact melt rocks. Pyroxene and olivine electron microprobe data for Oued Awlitis 001, poikilitic impact melt clasts in Shişr 161 (Wittmann et al. 2014b), an "intergranular clast" in PCA 02007 (arrow and compositional range; Korotev et al. 2006), pyroxene in a "basaltic clast" in NWA 7948 (Zeng et al. 2018), and poikilitic "matrix" pyroxene and olivine in NWA 482 (Daubar et al. 2002); note that Warren et al. (2005) report typical olivine compositions of $Fo_{64.2–66.7}$ for NWA 482.

may indicate a different origin on the Moon from OA 001. Additional measurements of ^{41}Ca (half-life = 0.104 Ma) in NWA 482 supersede a previous exposure age estimation by Nishiizumi and Caffee (2001) and determined an ejection age of NWA 482 of 0.29 Ma from a ~240 g cm^{-2} depth in the Moon (Nishiizumi 2003).

Additionally, several lunar meteorites contain clasts of melt rocks with poikilitic textures similar to that in OA 001.

1. NWA 7022 contains a ~4 cm impact melt rock clast that displays a poikilitic texture although it is far more enriched in incompatible elements than OA 001 (e.g., 0.70 wt% Na_2O; 3 ppm Th; Kuehner et al. 2012). The pyroxene oikocrysts and olivine clasts in this melt rock fall in the same compositional range as the pyroxene and olivine oikocrysts in OA 001; phenocryst plagioclase, however, is much more enriched in Na and K in this melt rock clast in NWA 7022 compared to phenocryst plagioclase in OA 001. Moreover, the impact melt rock clast in NWA 7022 contains accessory baddeleyite, armalcolite, merrillite, and zircon that we have not observed in OA 001.
2. Pecora Escarpment (PCA) 02007 contains a 1.4 mm poikilitic melt rock clast that Korotev et al. (2006) described in their fig. 5a as an "intergranular lithic clast." The mineral components in this clast fall in the range of compositions of the mineral components of OA 001.
3. We previously identified two clasts in lunar meteorite Shişr 161 with a poikilitic texture comparable to OA 001 (fig. 6b in Wittmann et al. 2014b).
4. Olivine and pyroxene compositions of OA 001, NWA 482, and clasts in Shişr 161 and PCA 02007 (Fig. 9) occupy the same compositional space, as do their plagioclase compositions ($An_{95–98}$) with the exception of a clast in OA 001 that is notably more sodic ($An_{88–89}$).
5. Zeng et al. (2018) reported a 0.4 × 0.7 mm "basaltic clast" in lunar regolith breccia meteorite NWA 7948 (clast "B5" in their fig. 2d) with a poikilitic texture akin the one of OA 001 and the abovementioned specimen. Plagioclase compositions of this clast ($An_{93.0–93.7}$ $Ab_{6.1–6.8}$ $Or_{0.2–0.3}$) contain notably more Na than the range of phenocryst plagioclase compositions in OA 001 ($An_{94.3–97.3}$) but lie within the range of clast-plagioclase compositions in OA 001 ($An_{88.1–97.9}$). Reported pyroxene compositions ($Fs_{41.6–53.0}$) of this clast are distinctly more ferroan than the pyroxene in OA 001 ($Fs_{19.6–41.7}$) but the Ca contents ($Wo_{17.4–33.9}$) fall within the range of OA 001 augite ($Wo_{6.4–34.0}$); Zeng et al. (2018) did not report olivine in this clast.

6. Joy et al. (2014) showed a "fine-grained poikilitic crystalline impact melt breccia" clast in lunar meteorite Sayh al Uhaymir 449 (clast 58 in their fig. 3l); however, no chemical data are available for this clast.
7. In lunar meteorite Sayh al Uhaymir 300, Hudgins et al. (2007) showed "an impact melt clast with a high proportion of mafics" in their fig. 3f, which is approximately 350 μm in size and has a poikilitic texture of plagioclase laths enclosed in pyroxene and olivine oikocrysts; no chemical information is available for this clast.

Rare earth element concentrations of OA 001 and NWA 482 are very similar and reasonably close to those of a poikilitic clast in Shişr 161 (Fig. 7). However, major element concentrations of OA 001 are distinct from NWA 482 and the poikilitic clasts in Shişr 161 (Fig. 6). Together, we think that these data suggest that OA 001 is unlikely a compositional pair to NWA 482 or the poikilitic clasts in Shişr 161.

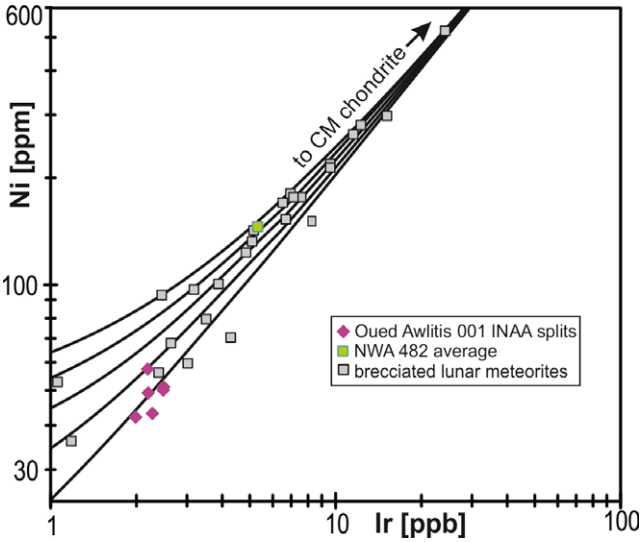

Fig. 10. Concentrations of Ni and Ir in lunar meteorites after Korotev (2012). Mean concentrations for brecciated lunar meteorites from Oman from Korotev (2012) and NWA 482 from Korotev et al. (2003). The curved lines are mixing lines between the bulk composition of CM chondrites (595 ppb Ir, 12000 ppm Ni; Wasson and Kallemeyn 1988) and low-Ir, low-Ni points (off scale) representing lunar silicates. Five lines are shown representing compositions at 0.01 ppb Ir and 5, 15, 25, 35, and 45 ppm Ni. The Ir concentration of OA 001, 2.3 ppb (0.4% CM chondrite equivalent), is at the low end of the range for feldspathic lunar meteorites (fig. 2a in Korotev et al. 2003), most of which are regolith and fragmental breccias.

Petrogenesis of OA 001

If OA 001 crystallized from an impact melt volume >100 m thick, scaling relationships suggest it must have been part of an impact crater >50 km in diameter (Cintala and Grieve 1998a, 1998b) or ponded melt in close proximity to a large crater. Moreover, its texture indicates that it is unlikely OA 001 underwent fractional crystallization (Wittmann et al. 2014b). Accordingly, it may be representative of the composition of a crustal, ferroan anorthositic target rock section. Whole-rock abundances of Ni and Ir in OA 001 suggest the presence of an impactor component admixed to a target component with very low concentrations of indigenous siderophile elements. Notably, while these data cannot be used to identify an impactor type, the indigenous component in OA 001 is different from the target component for NWA 482 (Fig. 10).

Tentatively, Ni and Co concentrations of kamacite in OA 001 are identical to those in L-chondrite kamacite (Fig. 11), which we also observed for kamacite compositions of inclusions in crystallized melt clasts and metal clasts in regolith breccia Shişr 161 (Wittmann and Korotev 2013). This observation substantiates that OA 001 is an impact melt rock (cf. Ryder et al. 1980; Warren 1993). However, for a conclusive identification of impactor type, elemental ratios of highly siderophile elements are required (e.g., Tagle and Berlin 2008).

Provenance of OA 001 on the Moon

Because OA 001 was launched from a depth of at least ~4 m and is not a regolith breccia, the present surface composition of the Moon may not necessarily be a good indicator for its provenance. However, we hypothesize that if the bulk composition of OA 001 is grossly representative of the regional composition of the uppermost lunar crust from which it formed, a comparison with the current composition of the uppermost lunar surface could still be useful. In this case, OA 001 could have been excavated by a secondary impact to a depth of ~4 m into an impact ejecta deposit, from where it was subsequently launched by another impact. To account for this scenario, we did least-squares comparison of OA 001's bulk rock composition (Table 1) with the Lunar Prospector's 5° γ-ray spectrometer data (Prettyman et al. 2006). Previously, this technique has been used to constrain the provenances of regolith breccias on the Moon's surface (e.g., Joy et al. 2010, 2011; Jolliff et al. 2014; Wittmann et al. 2014b; Calzada-Diaz et al. 2015; Zeng et al. 2018). Our match algorithm compared Lunar Prospector 5° γ-ray spectrometer data to that of OA 001, computed an error-weighted sum of squares of differences, and divided this result by the number of components to give a reduced χ^2/ν value. The best matches (reduced $\chi^2/\nu \leq 1$) are shown in Fig. 12 and indicate a clustering in a broad band between lunar latitudes of 45 to −65° and longitudes of 182.5 to 296°

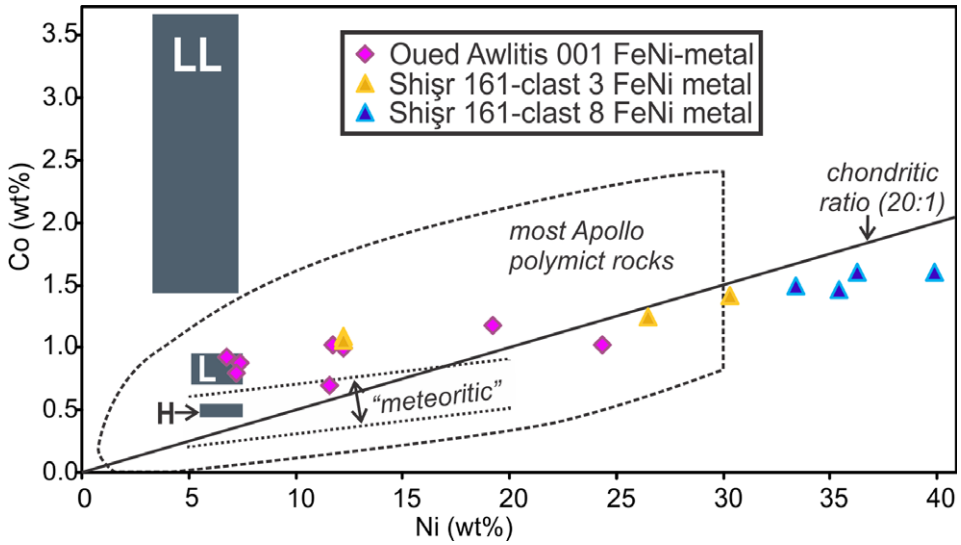

Fig. 11. Compositions of FeNi metal particles in lunar poikilitic impact melt rocks. Fields for most Apollo polymict rocks ("range of metal compositions in most polymict rocks") after Ryder et al. (1980); "meteoritic" field after Goldstein and Yakowitz (1971), ranges of equilibrated ordinary chondrite kamacite compositions after Rubin (1990); compositions of poikilitic melt clasts 3 and 8 in lunar meteorite Shişr 161 after Wittmann et al. (2014b); all data normalized to 100 wt%.

on the lunar surface (Table S7 in supporting information). The best-matched region (reduced $\chi^2/\nu = 0.4$) between the composition of OA 001 and the Lunar Prospector 5° γ-ray spectrometer data lies in Orientale impact basin's western Inner Rook Ring.

Launch Constraints for OA 001

OA 001 could have been launched from the Moon by an impact that excavated it from where it had crystallized. Excavation of material from a depth of 50–100 m on the Moon can be accomplished by relatively small impacts that produce craters with final diameters of 1–3 km and occur at a frequency of a several dozen per Ma (Warren 1994). However, to accelerate ejecta to the escape velocity from the Moon, the meteoritic material must have been part of a spall zone. Warren (1994) assumed that this "shock wave interference zone" is expected to be on the order of 50 m thick in a solid crystalline target rock for a 10 km diameter crater on the Moon. In addition, our CRE data indicate the crater that ejected OA 001 from the Moon formed 0.3 Ma ago. Thus, we expect a very limited number of candidate impact sites on the Moon for this launch scenario of OA 001 because impacts that could produce a 10 km diameter crater on the Moon have a statistical occurrence of one every 1–4 Ma, and impacts that could produce a ~20 km diameter crater only have a probability to form every 4–15 Ma (Neukum and Ivanov 1994; Warren 1994; Withers 2001).

Alternatively, OA 001 could have been launched as a component embedded in regolith. Hence, OA 001 would have been excavated from a minimum depth of 50 m—the center of a 100 m thick impact melt volume—by an impact that produced a > 0.5 km diameter crater. OA 001 would have subsequently been part of an ejecta blanket on the Moon, deposited at a depth of at least ~4 m before it was launched into an Earth-crossing orbit by a third impact. This third impact likely produced a crater larger than 5 km in diameter, owing to the relatively lower compressional shear velocity of porous regolith compared to solid crystalline rock (Warren 1994). However, it is uncertain if the event that produced the ~20 GPa pressure pulse in OA 001 and presumably excavated it was overprinted by another shock event that could have launched OA 001. Multiple shock events would likely have caused extensive brittle damage to the delicate, glassy shock melt veins and pockets in OA 001 (Fig. 4), which is not evident.

Candidate Launch Sites

Launch from Shallow Depth as a Regolith Component

If OA 001 has been a component of an ejecta blanket, a small impact that produced a crater only a few km in diameter could have ejected it from the Moon. If the composition of OA 001 is representative for the composition of the near-surface region from where it was ejected, Fig. 12 could be useful to identify very young impact events in high-resolution images of regions on the Moon that best-matched the composition of OA 001. We examined LROC Wide-Angle Camera (WAC) images

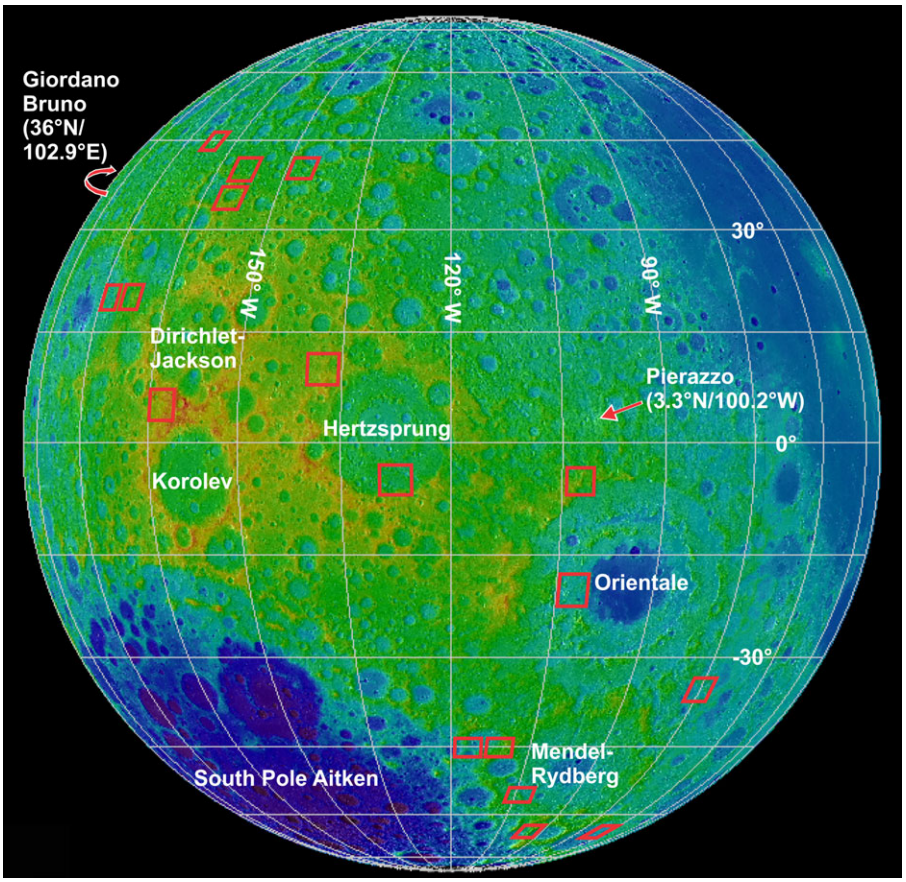

Fig. 12. Least-squares matching calculations of Oued Awlitis 001 with Lunar Prospector 5° γ-ray spectrometer data. The 17 best matches (reduced χ^2/ν <1) of matching calculations are shown as red squares on a projection of the WAC GLD100 digital terrain model (Scholten et al. 2012) overlain on the WAC 100 mpp global morphology mosaic. Major impact basin names and young craters Giordano Bruno and Pierazzo are indicated.

using a the global morphology mosaic (100 mpp) overlain with Lunar Reconnaissance Orbiter Diviner normalized nighttime soil temperature data and rock abundance data for all 17 best-fit regions indicated by our least-squares matching calculations. The soil temperature data are normalized to remove latitude variations and show temperature differences with red indicating warmer than average, blue colder than average, and green average nighttime temperatures. Diviner rock abundance data illustrate modeling of the fraction of exposed rocks ≥1 m versus fine-grained regolith in a region based on day to night temperature differences (Bandfield et al. 2011) (Fig. S1 in supporting information). High rock abundances in lunar crater ejecta characterize young craters based on the assumption that micrometeorite impacts comminute rocks exposed on the Moon's surface over time (Ghent et al. 2014).

Seven of the regions of interest do not contain young impacts (Table S7), which would be indicated by high-positive nighttime temperature anomalies. Ten regions of interest do show such positive temperature anomalies that identify 19 small impact craters 0.5–5 km in diameter, consistent with previous observations of numerous small impacts on the lunar surface (Speyerer et al. 2016). The potentially youngest impact crater we identified within one of the regions of interest based on the extensive temperature anomaly associated with it is 2.5 km in diameter and formed near the NNE rim of Orientale basin (Fig. 13).

Another intriguing candidate launch site could be 9.3 km diameter Pierazzo crater (Bray et al. 2018) that displays a fresh ray system and a massive positive nighttime temperature anomaly (Figs. 13 and S1). Although the age of Pierazzo crater has not been well constrained outside its very fresh appearance, its location near several best-fit regions of interest and relatively low reduced χ^2/ν value of 4.8 suggest it is a reasonable candidate for the launch of debris from Orientale's ejecta blanket, in which OA 001 could have been an excavated component.

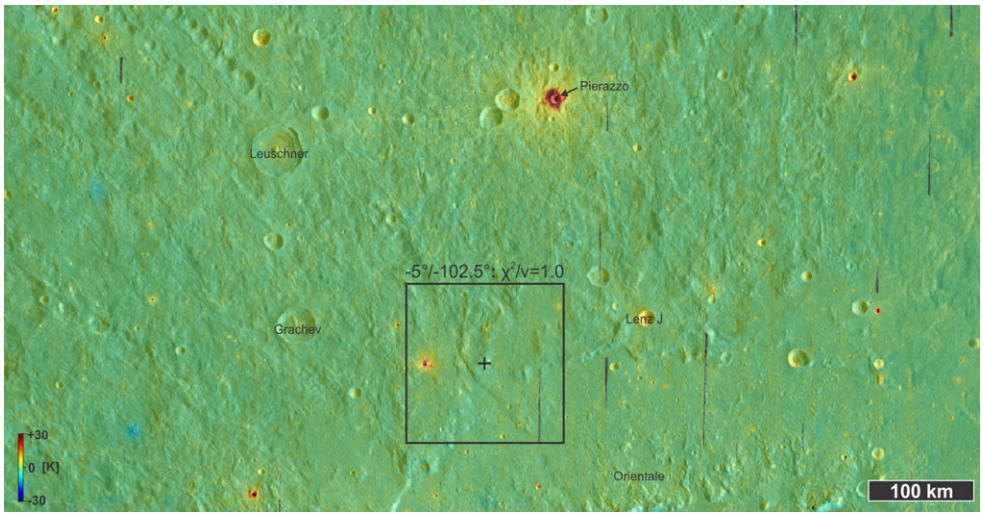

Fig. 13. Region of interest near N rim of Orientale impact basin. The 5° region with a reduced χ^2/ν of 1.0 centered at −5°/−102.5° is indicated as a black square on the Lunar Reconnaissance Orbiter Wide-Angle Camera mosaic basemap (100 mpp) that is overlain by color-coded Lunar Reconnaissance Orbiter Diviner normalized nighttime temperature data. Image is generated with NASA/GSFC/ASU-ACTREACT QuickMap (Robinson et al. 2010). Note fresh, 2.5 km wide impact crater that shows rays and a positive temperature anomaly near the E limit of the region of interest and massive temperature anomaly associated with Pierazzo crater.

Launch from Depth of Formation as a Crystallized Impact Melt Rock

The youngest lunar time unit is the Copernican Period whose base is defined by the rayed deposits of 93 km diameter Copernicus crater (Wilhelms 1987). The four youngest lunar rayed craters ≥18 km in diameter are 37 km diameter Necho, 18 km diameter Byrgius A, 24 km diameter Moore F, and 22 km diameter Giordano Bruno crater (Grier and McEwen 2001; Grier et al. 2001; IAU 2016). They have model ages from cumulative size-frequency distributions of craters counted on their continuous ejecta blankets of 80, 48, 41, and 4 Ma, respectively (Morota et al. 2009). These data are only consistent with Giordano Bruno crater (Fig. 14) as a candidate in this size group for the launch site of OA 001. Giordano Bruno crater has previously been implicated as the launch site for lunar meteorites Allan Hills 81005 (Ryder and Ostertag 1983), which has been launched 0.04–0.1 Ma ago (Nishiizumi et al. 1991), and paired stones Yamato-82192/82193/86032 (Fritz 2012), which were launched 8 ± 3 Ma ago (Lorenzetti et al. 2005).

The Diviner Lunar Radiometric Experiment on board the Lunar Reconnaissance Orbiter (e.g., Paige et al. 2010; Ghent et al. 2014) measured the reflected visible and emitted infrared radiation of Giordano Bruno's ejecta. Minimal mechanical disruption by micrometeoroid impacts is indicated by the heterogeneity of these data, which are, thus, consistent with a formation age of Giordano Bruno of <10 Ma (Williams et al. 2016). Ultraviolet spectral properties that record high reflectance commensurate with low degrees of space weathering (Denevi et al. 2014) furthermore confirm the relative freshness of Giordano Bruno ejecta. Further constraints for the age of Giordano Bruno to 5–10 Ma have been based on presumed secondary craters at the Luna 24 landing site (Basilevsky and Head 2012). However, Plescia et al. (2010) suggested Giordano Bruno could be much younger, even historical (cf. Hartung 1976), because self-secondary craters may yield artificially old crater counting ages with discrepancies between counts on the ejecta blanket and impact melt surfaces (Zanetti et al. 2017). Williams et al. (2014) presented crater counting ages for Giordano Bruno that take self-secondary craters into account and find ages as low as 0.61 Ma, which agrees with estimates by Shkuratov et al. (2012) for an age on the order of 1 Ma based on optical roughness imagery. Consequently, we conclude that the age of Giordano Bruno may not be conclusively older than our CRE age constraints for OA 001.

Giordano Bruno did not form on the melt sheet of a large impact crater. However, it is located just outside the southeastern rim of 337 km diameter pre-Nectarian Harkhebi crater, which has recently been identified as a peak ring basin on the basis of its gravity signature (Neumann et al. 2015). It is also within one crater radius of 122 km diameter Szilard crater to the southeast (IAU 2016; Fig. 14A). Topography data for Giordano Bruno produced from the high-resolution narrow-angle camera on board the Lunar Reconnaissance Orbiter reveal steep walls (Fig. 14B).

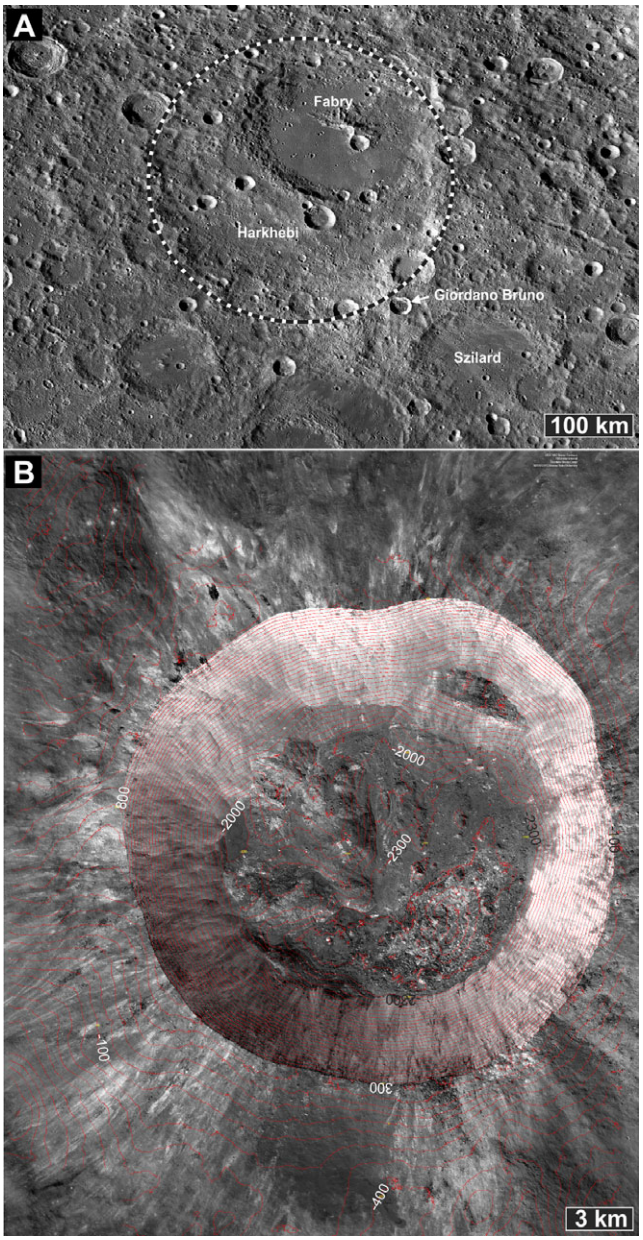

Fig. 14. Giordano Bruno crater. A) Regional context for Giordano Bruno crater from NASA/GSFC/ASU-ACT-REACT QuickMap. Approximate outline for Harkhebi basin redrawn after IAU (2016). B) LROC NAC mosaic with contour lines generated from stereo observations at a resolution of 50 cm (NASA/GSFC/Arizona State University).

While all crater walls have a relief greater than 2 km, the northwestern wall displays ~2.8 km steep walls with angles of 40 degrees, suggesting solid rocks near the surface. This observation could indicate ponded impact melt near the crater rim of Harkhebi. Such ponded impact melt deposits are known from many smaller lunar craters but typically only amount to a few decameters in thickness, at most (Zanetti et al. 2011; Öhman and Kring 2012). Denevi et al. (2012) derived a maximum thickness of 26 m for impact melt flows associated with 15 km diameter Mandel'shtam F crater. Thus, it seems plausible that ponded impact melt near the rim of 337 km diameter Harkhebi crater could have had a thickness of ~100 m. Our least-squares matching calculation for the region that includes Giordano Bruno with the composition of OA 001 indicates a reduced χ^2/ν of 11 and, thus, a poor fit. Moreover, if Giordano Bruno launched OA 001, we would expect many more lunar meteorites with similar ejection ages as OA 001 (cf. Fritz 2012). This circumstance may require more cosmogenic nuclide studies of lunar meteorites to reach a statistically robust conclusion.

Implications for the Ages of OA 001's Crystallization and Shock Melts

We think radioisotopic age dating experiments could be useful to test our hypotheses that OA 001 was launched during the formation of Giordano Bruno crater (Fig. 14), Pierazzo crater (Fig. 13), or a small crater on the Moon's farside (Fig. 12).

1. A pre-Nectarian age older than ~3.92 Ga (Stöffler et al. 2006) for the crystallization of the poikilitic impact melt rock OA 001 could point toward a connection with Giordano Bruno, which may have launched ponded impact melt from Harkhebi crater.
2. If poikilitic impact melt rock OA 001 has an age of ~3.7 Ga, impact-processing during the formation of Orientale basin could be indicated (Stöffler et al. 2006; Povilaitis et al. 2018) with a subsequent launch by the impact that formed Pierazzo crater.
3. If formation ages of the poikilitic impact melt rock are determined that postdate the formation of Orientale basin, and thus, the basin-forming eon of the Moon, launch sites characterized by small recent impact craters on the Moon's farside are probable launch sites for OA 001 (Fig. 12; Table S7).
4. If ages for the shock melt veins and pockets in OA 001 are determined, we can distinguish between their formation during launch approximately 0.3 Ma ago, or during excavation and subsequent incorporation into the lunar megaregolith if an age substantially older than ~0.3 Ma is found.

However, we anticipate that a radioisotopic age dating experiment will be complicated because of the clast-rich nature of OA 001 and its low abundance of incompatible elements with radioactive isotopes suitable for the determination of an absolute age (e.g., 0.03 wt% K_2O, 0.08 ppm of U, 0.214 ppm of Th; Table 1).

CONCLUSIONS

Lunar meteorite OA 001 is a clast-rich, poikilitic impact melt rock. Texturally and compositionally similar lithologies constitute lunar meteorite NWA 482 and clast components in other lunar meteorites. The chemistry of OA 001 suggests it formed from a ferroan anorthositic precursor rock with little (if any) addition of incompatible-element-enriched components. Its cosmogenic nuclide inventory indicates it was launched about 0.3 Ma ago from a depth of at least 4 m on the Moon and experienced little ablation during its passage through Earth's atmosphere. Although we could not determine its terrestrial residence time because of a high content of solar cosmic ray-produced nuclides, OA 001 is a fresh stone with a mostly intact fusion crust and little evidence for terrestrial alteration.

Its petrology suggests that OA 001 and texturally similar rocks formed in an impact melt volume more than 100 m thick, which typically occur in craters larger than about 50 km in diameter on the Moon. If OA 001 was launched by the impact that excavated it, only the youngest large lunar impact craters are potential launch sites. A possible launch crater is Giordano Bruno. However, a relative scarcity of launch-paired lunar meteorites weaken the case for a 0.3 Ma age of Giordano Bruno.

Using least-squares calculations that compare the Lunar Prospector's 5° γ-ray spectrometer data with the bulk composition of OA 001 indicate best matches with a relatively limited region on the lunar farside. A survey of these best match regions with high-resolution Lunar Reconnaissance Orbiter imagery and Diviner nighttime temperature data identifies several young impact craters up to 5 km in diameter. The impacts that created these craters may not have been sufficient to launch OA 001 from the regolith, though. In contrast, 9.3 km diameter Pierazzo crater, which formed on the ejecta blanket of Orientale, appears very young and may thus be a candidate for the launch of OA 001.

Acknowledgments—We gratefully acknowledge funding by NASA grant NNX14AK62G to KN, NNX14AI65G to RLK, and LRO contract NNG07EK00C via GSFC and ASU to BLJ, support from the McDonnell Center for the Space Sciences, and the use of the electron microprobe laboratories at the Department of Earth and Planetary Sciences of Washington University in St. Louis and Arizona State University's Eyring Materials Center. Paul Carpenter (Washington University in St. Louis) assisted with electron microprobe analyses. Mohamed Aid and Zaid Oussaid recovered Oued Awlitis 001. Jörg Fritz (Saalbau Weltraum Projekt Heppenheim) discussed implications for the age of Giordano Bruno crater. Katherine Joy (University of Manchester, UK) pointed out some poikilitic melt rock clasts in lunar meteorites and reviewed this manuscript. We also thank reviewers Natalie Curran (NASA Goddard Space Flight Center) and John Spray (University of New Brunswick) for helpful reviews and associate editors Christian Koeberl and Katherine Joy for handling the manuscript. A. W. thanks Uwe Reimold for past guidance and inspiration for his studies of impact rocks.

Editorial Handling—Dr. Katherine Joy

REFERENCES

Abramov O. and Kring D. A. 2004. Numerical modeling of an impact-induced hydrothermal system at the Sudbury crater. *Journal of Geophysical Research* 109:E10007. https://doi.org/10.1029/2003je002213.

Abramov O. and Kring D. A. 2007. Numerical modeling of impact-induced hydrothermal activity at the Chicxulub crater. *Meteoritics & Planetary Science* 42:93–112. https://doi.org/10.1111/j.1945-5100.2007.tb00220.x.

Anders E. and Grevesse N. 1989. Abundances of the elements: Meteoritic and solar. *Geochimica et Cosmochimica Acta* 53:197–214. https://doi.org/10.1016/0016-7037(89)90286-X.

Ashley J. W., Robinson M. S., Hawke B. R., Van der Bogert C. H., Hiesinger H., Sato H., Speyerer E. J., Enns A. C., Wagner R. V., Young K. E., and Burns K. N. 2012. Geology of the King crater region: New insights into impact melt dynamics on the Moon. *Journal of Geophysical Research* 117: E00H29. https://doi.org/10.1029/2011je003990.

Ashley J. W., Robinson M. S., Stopar J. D., Glotch T. D., Hawke B. R., Van der Bogert C. H., Hiesinger H., Lawrence S. J., Jolliff B. L., Greenhagen B. T., Giguere T. A., and Paige D. A. 2016. The Lassell massif—A silicic lunar volcano. *Icarus* 273:248–261. https://doi.org/10.1016/j.icarus.2015.12.036.

Bandfield J. L., Ghent R. R., Vasavada A. R., Paige D. A., Lawrence S. J., and Robinson M. S. 2011. Lunar surface rock abundance and regolith fines temperatures derived from LRO Diviner Radiometer data. *Journal of Geophysical Research* 116:E00H02. https://doi.org/10.1029/2011je003866.

Basilevsky A. T. and Head J. W. 2012. Age of Giordano Bruno crater as deduced from the morphology of its secondaries at the Luna 24 landing site. *Planetary and Space Science* 73:302–309. https://doi.org/10.1016/j.pss.2012.08.017.

Beran A. and Koeberl C. 1997. Water in tektites and impact glasses by fourier-transformed infrared spectrometry. *Meteoritics & Planetary Science* 32:211–216. https://doi.org/10.1111/j.1945-5100.1997.tb01260.x.

Braden S. E., Stopar J. D., Robinson M. S., Lawrence S. J., Van der Bogert C. H., and Hiesinger H. 2014. Evidence for basaltic volcanism on the Moon within the past 100 million years. *Nature Geosciences* 7:787–791. https://doi.org/10.1038/NGEO2252.

Bray V. J., Tornabene L. L., Keszthelyi L. P., McEwen A. S., Hawke B. R., Giguere T. A., Kattenhorn S. A., Garry W. B., Rizk B., Caudill C. M., Gaddis L. R., and Van der Bogert C. H. 2010. New insights into lunar impact melt mobility from the LRO camera. *Geophysical Research Letters* 37:L21202. https://doi.org/10.1029/2010GL044666.

Bray V. J., Atwood-Stone C., Neish C. D., Artemieva N. A., McEwen A. S., and McElwaine J. N. 2018. Lobate impact

melt flows within the extended ejecta blanket of Pierazzo crater. *Icarus* 301:26–36. https://doi.org/10.1016/j.icarus.2017.10.002.

Cahill J. T. S., Thomson B. J., Patterson G. W., Benjamin D., Bussey J., Neish C. D., Lopez N. R., Turner F. S., Aldridge T., McAdam M., Meyer H. M., Raney R. K., Carter L. M., Spudis P. D., Hiesinger H., and Pasckert J. H. 2014. The Miniature Radio Frequency instrument's (Mini-RF) global observations of Earth's Moon. *Icarus* 243:173–190. https://doi.org/10.1016/j.icarus.2014.07.018.

Calzada-Diaz A., Joy K. H., Crawford I. A., and Nordheim T. A. 2015. Constraining the source regions of lunar meteorites using orbital geochemical data. *Meteoritics & Planetary Science* 50:214–228. https://doi.org/10.1111/maps.12737.

Calzada-Diaz A., Joy K. H., Crawford I. A., and Strekopytov S. 2016. The petrology, geochemistry, and age of lunar regolith breccias Miller Range 090036 and 090070: Insights into the crustal history of the Moon. *Meteoritics & Planetary Science* 52:3–23. https://doi.org/10.1111/maps.12737.

Cassanelli J. P. and Head J. W. 2016. Did the Orientale impact melt sheet undergo large-scale igneous differentiation by crystal settling? *Geophysical Research Letters* 43:11,156–11,165. https://doi.org/10.1002/2016GL070425.

Cintala M. J. and Grieve R. A. F. 1998a. Scaling impact melting and crater dimensions: Implications for the lunar cratering record. *Meteoritics & Planetary Science* 33:889–912. https://doi.org/10.1111/j.1945-5100.1998.tb01695.x.

Cintala M. J. and Grieve R. A. F. 1998b. Scaling impact melting and crater dimensions: Implications for the lunar cratering record—Errata. *Meteoritics & Planetary Science* 33:1343. https://doi.org/10.1111/j.1945-5100.1998.tb01320.x.

Clark J. D., Hurtado J. M. Jr., Hiesinger H., Van der Bogert C. H., and Bernhardt H. 2017. Investigation of newly discovered lobate scarps: Implications for the tectonic and thermal evolution of the Moon. *Icarus* 298:78–88. https://doi.org/10.1016/j.icarus.2017.08.017.

Daubar I. J., Kring D. A., Swindle T. D., and Jull A. J. T. 2002. Northwest Africa 482: A crystalline impact-melt breccia from the lunar highlands. *Meteoritics & Planetary Science* 37:1797–1813. https://doi.org/10.1111/j.1945-5100.2002.tb01164.x.

Delano J. W., Bence A. E., Papike J. J., and Cameron K. L. 1973. Petrology of the 2-4 mm soil fraction from the Descartes region of the Moon and stratigraphic implications. Proceedings, 4th Lunar Science Conference. pp. 537–551.

Denevi B. W., Koeber S. D., Robinson M. S., Garry W. B., Hawke B. R., Tran T. N., Lawrence S. J., Keszthelyi L. P., Barnouin O. S., Ernst C. M., and Tornabene L. L. 2012. Physical constraints on impact melt properties from Lunar Reconnaissance Orbiter Camera images. *Icarus* 219:665–675. https://doi.org/10.1016/j.icarus.2012.03.020.

Denevi B. W., Robinson M. S., Boyd A. K., Sato H., Hapke B. W., and Hawke B. R. 2014. Characterization of space weathering from Lunar Reconnaissance Orbiter Camera ultraviolet observations of the Moon. *Journal of Geophysical Research: Planets* 119:976–997. https://doi.org/10.1002/2013JE004527.

Donahue D. J., Jull A. J. T., and Linick T. W. 1990a. Isotope-ratio and background corrections for accelerator mass spectrometry radiocarbon measurements. *Radiocarbon* 32:135–142. https://doi.org/10.2458/azu_js_rc.32.1261.

Donahue D. J., Jull A. J. T., and Toolin L. J. 1990b. Radiocarbon measurements at the University of Arizona AMS facility. *Nuclear Instruments and Methods in Physics Research* B52:224–228. https://doi.org/10.1016/0168-583X(90)90410-V.

Ferrière L., Meier M. M. M., Assis Fernandes V., Fritz J., Greshake A., Barrat J.-A., Böttger U., Bouvier A., Brandstätter F., Busemann H., Korotev R. L., Maden C., Magna T., Schmitt-Kopplin Ph., Schrader D. L., and Wadhwa M. 2017. The unique crowdfunded Oued Awlitis 001 lunar meteorite—A consortium overview (abstract #1621). 48th Lunar and Planetary Science Conference. CD-ROM.

Floran R. J., Grieve R. A. F., Phinney W. C., Warner J. L., Simonds C. H., Blanchard D. P., and Dence M. R. 1978. Manicouagan impact melt, Quebec, 1, Stratigraphy, petrology, and chemistry. *Journal of Geophysical Research* 83:2737–2759. https://doi.org/10.1029/JB083iB06p02737.

Fritz J. 2012. Impact ejection of lunar meteorites and the age of Giordano Bruno. *Icarus* 221:1183–1186. https://doi.org/10.1016/j.icarus.2012.08.019.

Fritz J., Wünnemann K., Reimold W. U., Meyer C., and Hornemann U. 2011. Shock pressure calibration for lunar plagioclase (abstract #1196). 42nd Lunar and Planetary Science Conference. CD-ROM.

Fritz J., Greshake A., and Fernandes V. A. 2017. Revising the shock classification of meteorites. *Meteoritics & Planetary Science* 52:1216–1232. https://doi.org/10.1111/maps.12845.

Ghent R. R., Hayne P. O., Bandfield J. L., Campbell B. A., Allen C. C., Carter L. M., and Paige D. A. 2014. Constraints on the recent rate of lunar ejecta breakdown and implications for crater ages. *Geology* 42:1059–1062. https://doi.org/10.1130/G35926.1.

Ghent R. R., Carter L. M., Bandfield J. L., Tai Udovicic C. J., and Campbell B. A. 2016. Lunar crater ejecta: Physical properties revealed by radar and thermal infrared observations. *Icarus* 273:182–195. https://doi.org/10.1016/j.icarus.2015.12.014.

Goldstein J. I. and Yakowitz H. 1971. Metallic inclusions and metal particles in the Apollo 12 lunar soil. Proceedings, 2nd Lunar Science Conference. pp. 177–191.

Greenhagen B. T., Neish C. D., Williams J.-P., Cahill J. T. S., Ghent R. R., Hayne P. O., Lawrence S. J., Petro N. E., and Bandfield J. L. 2016. Origin of the anomalously rocky appearance of Tsiolkovskiy crater. *Icarus* 273:237–247. https://doi.org/10.1016/j.icarus.2016.02.041.

Grier J. A. and McEwen A. S. 2001. The lunar record of recent impact cratering. In *Accretion of extraterrestrial matter throughout Earth's history*, edited by Peucker-Ehrenbrink B. and Schmitz B. New York: Kluwer Academic/Plenum Publishers. pp. 403–422. https://doi.org/10.1007/978-1-4419-8694-8_20.

Grier J. A., McEwen A. S., Lucey P. G., Milazzo M., and Strom R. G. 2001. Optical maturity of ejecta from large rayed lunar craters. *Journal of Geophysical Research* 106:32,847–32,862. https://doi.org/10.1029/1999JE001160.

Grieve R. A. F. 1975. Petrology and chemistry of the impact melt at Mistastin Lake crater, Labrador. *Geological Society of America Bulletin* 86:1617–1629. https://doi.org/10.1130/0016-7606(1975) 86 < 1617:PACOTI > 2.0.CO;2.

Grieve R. A. F., Stöffler D., and Deutsch A. 1991. The Sudbury structure: Controversial or misunderstood? *Journal of Geophysical Research* 96:22,753–22,764. https://doi.org/10.1029/91JE02513.

Hart R. J., Cloete M., McDonald I., Carlson R. W., and Andreoli M. A. G. 2002. Siderophile-rich inclusions from

the Morokweng impact melt sheet, South Africa: Possible fragments of a chondritic meteorite. *Earth and Planetary Science Letters* 198:49–62. https://doi.org/10.1016/S0012-821X(02)00497-1.

Hartung J. B. 1976. Was the formation of a 20-km-diameter impact crater on the Moon observed on June 18, 1178? *Meteoritics* 11:187–194.

Haskin L. A., Helmke P. A., Blanchard D. P., Jacobs J. W., and Telander K. 1973. Major and trace element abundances in samples from the lunar highlands. Proceedings, 4th Lunar Science Conference. pp. 1275–1296.

Hayne P. O., Bandfield J. L., Siegler M. A., Vasavada A. R., Ghent R. R., Williams J.-P., Greenhagen B. T., Aharonson O., Elder C. M., Lucey P. G., and Paige D. A. 2017. Global regolith thermophysical properties of the Moon from the Diviner lunar radiometer experiment. *Journal of Gephysical Research: Planets* 122:2371–2400. https://doi.org/10.1002/2017je005387.

Herzog G. F. and Caffee M. W. 2014. Cosmic-ray exposure ages of meteorites. In *Meteorites and cosmochemical processes*, 2nd ed., edited by Holland H. D. and Turekian K. K. Treatise on Geochemistry, vol. 1. Oxford: Elsevier. pp. 419–454. https://doi.org/10.1016/b978-0-08-095975-7.00110-8.

Hiesinger H., Van der Bogert C. H., Pasckert J. H., Funcke L., Giacomini L., Ostrach L. R., and Robinson M. S. 2012. How old are young lunar craters? *Journal of Geophysical Research* 117:E00H10. https://doi.org/10.1029/2011je003935.

Hudgins J. A., Walton E. L., and Spray J. G. 2007. Mineralogy, petrology, and shock history of lunar meteorite Sayh al Uhaymir 300: A crystalline impact-melt breccia. *Meteoritics & Planetary Science* 42:1763–1779. https://doi.org/10.1111/j.1945-5100.2007.tb00536.x.

IAU. 2016. International Astronomical Union Working Group for Planetary System Nomenclature—Gazetteer of Planetary Nomenclature. http://planetarynames.wr.usgs.gov/. (accessed December 13, 2016).

Jolliff B. L., Korotev R. L., and Haskin L. A. 1991. Geochemistry of 2-4-mm particles from Apollo 14 soil (14161) and implications regarding igneous components and soil-forming processes. Proceedings, 23rd Lunar and Planetary Science Conference. pp. 193–219.

Jolliff B. L., Gillis J. J., Haskin L. A., Korotev R. L., and Wieczorek M. A. 2000. Major lunar crustal terranes: Surface expressions and crust-mantle origins. *Journal of Geophysical Research* 105:4197–4216. https://doi.org/10.1029/1999JE001103.

Jolliff B. L., Carpenter P. K., Korotev R. L., North-Valencia S. N., Wittmann A., and Zeigler R. A. 2014. Connecting lunar meteorites to source terrains on the Moon (abstract). *Microscopy and Microanalysis* 20 (Supplement 3):1670–1671. https://doi.org/10.1017/s1431927614010083.

Joy K. H., Crawford I. A., Russell S. S., and Kearsley A. T. 2010. Lunar meteorite regolith breccias: An in situ study of impact melt composition using LA-ICP-MS with implications for the composition of the lunar crust. *Meteoritics & Planetary Science* 45:917–946. https://doi.org/10.1111/j.1945-5100.2010.01067.x.

Joy K. H., Burgess R., Hinton R., Fernandes V. A., Crawford I. A., Kearsley A. T., and Irving A. J., and EIMF. 2011. Petrogenesis and chronology of lunar meteorite Northwest Africa 4472: A KREEPy regolith breccia from the Moon. *Geochimica et Cosmochimica Acta* 75:2420–2452. https://doi.org/10.1016/j.gca.2011.02.018.

Joy K. H., Nemchin A., Grange M., Lapen T. J., Peslier A. H., Ross D. K., Zolensky M. E., and Kring D. A. 2014. Petrography, geochronology and source terrain characteristics of lunar meteorites Dhofar 925, 961 and Sayh al Uhaymir 449. *Geochimica et Cosmochimica Acta* 144:299–325. https://doi.org/10.1016/j.gca.2014.08.013.

Jull A. J. T., Cloudt S., Donahue D. J., Sisterson J. M., Reedy R. C., and Masarik J. 1998. ^{14}C depth profiles in Apollo 15 and 17 cores and lunar rock 6881. *Geochimica et Cosmochimica Acta* 62:3025–3036. https://doi.org/10.1016/S0016-7037(98)00193-8.

Kirchoff M. R., Chapman C. R., Marchi S., Curtis K. M., Enke B., and Bottke W. F. 2013. Ages of large lunar impact craters and implications for bombardment during the Moon's middle age. *Icarus* 225:325–341. https://doi.org/10.1016/j.icarus.2013.03.018.

Korotev R. L. 2005. Lunar geochemistry as told by lunar meteorites. *Chemie der Erde/Geochemistry* 65:297–346. https://doi.org/10.1016/j.chemer.2005.07.001.

Korotev R. L. 2012. Lunar meteorites from Oman. *Meteoritics & Planetary Science* 47:1365–1402. https://doi.org/10.1111/j.1945-5100.2012.01393.x.

Korotev R. L. 2017. Update (2012–2017) on lunar meteorites from Oman. *Meteoritics & Planetary Science* 52:1251–1256. https://doi.org/10.1111/maps.12869.

Korotev R. L., Jolliff B. L., Zeigler R. A., Gillis J. J., and Haskin L. A. 2003. Feldspathic lunar meteorites and their implications for compositional remote sensing of the lunar surface and the composition of the lunar crust. *Geochimica et Cosmochimica Acta* 67:4895–4923. https://doi.org/10.1016/j.gca.2003.08.001.

Korotev R. L., Zeigler R. A., and Jolliff B. L. 2006. Feldspathic lunar meteorites Pecora Escarpment 02007 and Dhofar 489: Contamination of the surface of the lunar highlands by post-basin impacts. *Geochimica et Cosmochimica Acta* 70:5935–5956. https://doi.org/10.1016/j.gca.2006.09.016.

Korotev R. L., Zeigler R. A., Jolliff B. L., Irving A. J., and Bunch T. E. 2009. Compositional and lithological diversity among brecciated lunar meteorites of intermediate iron concentration. *Meteoritics & Planetary Science* 44:1287–1322. https://doi.org/10.1111/j.1945-5100.2009.tb01223.x.

Kramer G. Y., Kring D. A., Nahm A. L., and Pieters C. M. 2013. Spectral and photogeologic mapping of Schrödinger Basin and implications for post-South Pole-Aitken impact deep subsurface stratigraphy. *Icarus* 223:131–148. https://doi.org/10.1016/j.icarus.2012.11.008.

Krüger T., Van der Bogert C. H., and Hiesinger H. 2016. Geomorphologic mapping of the lunar crater Tycho and its impact melt deposits. *Icarus* 273:164–181. https://doi.org/10.1016/j.icarus.2016.02.018.

Kuehner S. M., Irving A. J., and Korotev R. L. 2012. Petrology and composition of lunar meteorite Northwest Africa 7022: An unusually sodic anorthositic gabbroic impact melt breccia with compositional similarities to Miller Range 090036 (abstract #1524). 43rd Lunar and Planetary Science Conference. CD-ROM.

Lofgren G. E. 1977. Dynamic crystallization experiments bearing on the origin in impact-generated liquids. Proceedings, 8th Lunar Science Conference. pp. 2079–2095.

Lorenzetti S., Busemann H., and Eugster O. 2005. Regolith history of lunar meteorites. *Meteoritics & Planetary Science* 40:315–327. https://doi.org/10.1111/j.1945-5100.2005.tb00383.x.

Marion C. L. and Sylvester P. J. 2010. Composition and heterogeneity of anorthositic impact melt at Mistastin Lake crater, Labrador. *Planetary and Space Science* 58:552–573. https://doi.org/10.1016/j.pss.2009.09.018.

Masarik J. and Reedy R. C. 1994. Effects of bulk composition on nuclide production processes in meteorites. *Geochimica et Cosmochimica Acta* 58:5307–5317. https://doi.org/10.1016/0016-7037(94)90314-X.

Melosh H. J. and Artemieva N. 2004. How does tektite glass lose its water? (abstract #1723). 35th Lunar and Planetary Science Conference. CD-ROM.

Mercer C. N., Treiman A. H., and Joy K. H. 2013. New lunar meteorite Northwest Africa 2996: A window into farside lithologies and petrogenesis. *Meteoritics & Planetary Science* 48:289–315. https://doi.org/10.1111/maps.12056.

Meyer H. M., Denevi B. W., Boyd A. K., and Robinson M. S. 2016. The distribution and origin of lunar light plains around Orientale basin. *Icarus* 273:135–145.

Morota T., Haruyama J., Miyamoto H., Honda C., Ohtake M., Yokota Y., Matsunaga T., Hirata N., Demura H., Takeda H., Ogawa Y., and Kimura J. 2009. Formation age of the lunar crater Giordano Bruno. *Meteoritics & Planetary Science* 44: 1115–1120. https://doi.org/10.1111/j.1945-5100.2009.tb01211.x.

Neukum G. and Ivanov B. A. 1994. Crater size distribution and impact probabilities on Earth from lunar, terrestrial-planet, and asteroid cratering data. In *Hazards due to comets and asteroids*, edited by Gehrels T., Matthews M. S., and Schumann A. Tucson, Arizona: The University of Arizona Press. pp. 359–416.

Neumann G. A., Zuber M. T., Wieczorek M. A., Head J. W., Baker D. M. H., Solomon S. C., Smith D. E., Lemoine F. G., Mazarico E., Sabaka T. J., Goossens S. J., Melosh H. J., Phillips R. J., Asmar S. W., Konopliv A. S., Williams J. G., Sori M. M., Soderblom J. M., Miljković K., Andrews-Hanna J. C., Nimmo F., and Kiefer W. S. 2015. Lunar impact basins revealed by Gravity Recovery and Interior Laboratory measurements. *Science Advances* 1:10. https://doi.org/10.1126/sciadv.1500852.

Nishiizumi K. 2003. Exposure histories of lunar meteorites. Evolution of solar system materials: A new perspective from Antarctic meteorites, 104 (abstract). National Institute of Polar Research, Tokyo.

Nishiizumi K. 2004. Preparation of ^{26}Al AMS standards. *Nuclear Instruments and Methods in Physics Research* B223–B224:388–392. https://doi.org/10.1016/j.nimb.2004.04.075.

Nishiizumi K. and Caffee W. M. 2001. Exposure histories of lunar meteorites Dhofar 025, 026, and Northwest Africa 482. 64th Annual Meeting of the Meteoritical Society (abstract).

Nishiizumi K., Elmore D., Ma X. Z., and Arnold J. R. 1984a. ^{10}Be and ^{36}Cl depth profiles in an Apollo 15 drill core. *Earth and Planetary Science Letters* 70:157–163. https://doi.org/10.1016/0012-821X(84)90001-3.

Nishiizumi K., Klein J., Middleton R., and Arnold J. R. 1984b. ^{26}Al depth profile in Apollo 15 drill core. *Earth and Planetary Science Letters* 70:164–168. https://doi.org/10.1016/0012-821X(84)90002-5.

Nishiizumi K., Arnold J. R., Klein J., Fink D., Middleton R., Kubik P. W., Sharma P., Elmore D., and Reedy R. C. 1991. Exposure histories of lunar meteorites: ALHA81005, MAC88104, MAC88105, and Yamato791197. *Geochimica et Cosmochimica Acta* 55:3149–3155. https://doi.org/10.1016/0016-7037(91)90479-O.

Nishiizumi K., Arnold R. J., Caffee W. M., Finkel C. R., and Reedy C. R. 1992. Cosmic ray exposure histories of lunar meteorites Asuka-881757, Yamato-793169, and Calcalong Creek. In *Symposium on Antarctic meteorites*. Tokyo: National Institute of Polar Research. pp. 129–132.

Nishiizumi K., Imamura M., Caffee M. W., Southon J. R., Finkel R. C., and McAninch J. 2007. Absolute calibration of ^{10}Be AMS standards. *Nuclear Instruments and Methods in Physics Research* B258:403–413. https://doi.org/10.1016/j.nimb.2007.01.297.

Nishiizumi K., Arnold J. R., Kohl C. P., Caffee M. W., Masarik J., and Reedy R. C. 2009. Solar cosmic ray records in lunar rock 64455. *Geochimica et Cosmochimica Acta* 73:2163–2176. https://doi.org/10.1016/j.gca.2008.12.021.

Nishiizumi K., Caffee M. W., and Jull A. J. T. 2016. Large solar cosmic ray effects on Oued Awlitis 001 lunar meteorite and Northwest Africa 10134 shergottite (abstract #1669). 47th Lunar and Planetary Science Conference. CD-ROM.

Norris T. L., Gancarz A. J., Rokop D. J., and Thomas K. W. 1983. Half-life of ^{26}Al. Proceedings, 14th Lunar and Planetary Science Conference. *Journal of Geophysical Research* 88:B331–B333. https://doi.org/10.1029/jb088is01p0b331.

Öhman T. and Kring D. A. 2012. Photogeologic analysis of impact melt-rich lithologies in Kepler crater that could be sampled by future missions. *Journal of Geophysical Research* 117:E00H08. https://doi.org/10.1029/2011je003918.

Onorato P. I. K., Uhlmann D. R., and Simonds C. H. 1978. The thermal history of the Manicouagan impact melt sheet. *Journal of Geophysical Research* 83:2789–2798. https://doi.org/10.1029/JB083iB06p02789.

Orgel C., Michael G., Fassett C. I., Van der Bogert C. H., Riedel C., Kneissl C., and Hiesinger H. 2018. Ancient bombardment of the inner solar system: Reinvestigation of the "fingerprints" of different impactor populations on the lunar surface. *Journal of Geophysical Research: Planets* 123:748–762. https://doi.org/10.1002/2017je005451.

Paige D. A., Foote M. C., Greenhagen B. T., Schofield J. T., Calcutt S., Vasvada A. R., Preston D. J., Taylor F. W., Allen C. C., Snook K. J., Jakoskoy B. M., Murray B. C., Soderblom L. A., Jau B., Loring S., Bulharowski J., Bowles N. E., Thomas I. R., Sullivan M. T., Avis C., De Jong E. M., Hartford W., and McCleese D. J. 2010. The Lunar Reconnaissance Orbiter Diviner Lunar Radiometer Experiment. *Space Science Reviews* 150:125–160. https://doi.org/10.1007/s11214-009-9529-2.

Papike J. J. 1998. Comparative planetary mineralogy: Chemistry of melt-derived pyroxene, feldspar, and olivine. In *Planetary materials*, vol. 36, edited by Papike J. J. Washington, D.C.: Mineralogical Society of America. pp. 7-01–7-12

Papike J. J., Ryder G., and Shearer C. K. 1998. Lunar samples. In *Planetary materials*, edited by Papike J. J. Washington, D.C.: Mineralogical Society of America. pp. 5-001–5-234.

Pickersgill A. E., Osinski G. R., and Flemming R. L. 2015. Shock effects in plagioclase feldspar from the Mistastin Lake impact structure, Canada. *Meteoritics & Planetary Science* 50:1546–1561. https://doi.org/10.1111/maps.12495.

Plescia J. B. and Cintala M. J. 2012. Impact melt in small lunar highland craters. *Journal of Geophysical Research* 117:E00H12. https://doi.org/10.1029/2011je003941.

Plescia J. B. and Spudis P. D. 2014. Impact melt flows at Lowell crater. *Planetary and Space Science* 103:219–227. https://doi.org/10.1016/j.pss.2014.08.003.

Plescia J. B., Robinson M. S., and Paige D. A. 2010. Giordano Bruno: The young and the restless (abstract #2038). 41st Lunar and Planetary Science Conference. CD-ROM.

Povilaitis R. Z., Robinson M. S., Van der Bogert C. H., Hiesinger H., Meyer H. M., and Ostrach L. R. 2018. Crater density differences: Exploring regional resurfacing, secondary crater populations, and crater saturation equilibrium on the Moon. *Planetary and Space Sciences* 162:41–51. https://doi.org/10.1016/j.pss.2017.05.006.

Prettyman T. H., Hagerty J. J., Elphic R. C., Feldman W. C., Lawrence D. J., McKinney G. W., and Vaniman D. T. 2006. Elemental composition of the lunar surface: Analysis of gamma ray spectroscopy data from Lunar Prospector. *Journal of Geophysical Research* 111:E12007. https://doi.org/10.1029/2005JE002656.

Robinson M. S., Brylow S. M., Tschimmel M., Humm D., Lawrence S. J., Thomas P. C., Denevi B. W., Bowman-Cisneros E., Zerr J., Ravine M. A., Caplinger M. A., Ghaemi F. T., Schaffner J. A., Malin M. C., Mahanti P., Bartels A., Anderson J., Tran T. N., Eliason E. M., McEwen A. S., Turtle E., Jolliff B. L., and Hiesinger H. 2010. Lunar Reconnaissance Orbiter Camera (LROC) instrument overview. *Space Science Reviews* 150:81–124. https://doi.org/10.1007/s11214-010-9634-2.

Robinson M. S., Thomas P. C., Plescia J. B., Denevi B. W., Burns K. N., Bowman-Cisneros E., Henriksen M. R., Van der Bogert C. H., Hiesinger H., Mahanti P., Stelling R. W., and Povilaitis R. Z. 2016. An exceptional grouping of lunar highland smooth plains: Geography, morphology, and possible origins. *Icarus* 273:121–134. https://doi.org/10.1016/j.icarus.2015.06.028.

Rollinson H. R. 1993. *Using geochemical data: Evaluation, presentation, interpretation*. London: Longman Scientific and Technical. p. 352.

Rubin A. E. 1990. Kamacite and olivine in ordinary chondrites: Intergroup and intragroup relationships. *Geochimica et Cosmochimica Acta* 54:1217–1232. https://doi.org/10.1016/0016-7037(90)90148-E.

Ruzicka A., Grossman J., Bouvier A., and Agee C. B. 2017. The Meteoritical Bulletin, No. 103. *Meteoritics & Planetary Science* 52:1014. https://doi.org/10.1111/maps.12888.

Ryder G. and Bower J. F. 1976. Poikilitic KREEP impact melts in the Apollo 14 white rocks. Proceedings, 7th Lunar Science Conference. pp. 1925–1948.

Ryder G. and Ostertag R. 1983. ALHA 81005: Moon, Mars, Petrography, and Giordano Bruno. *Geophysical Research Letters* 10:791–794. https://doi.org/10.1029/GL010i009p00791.

Ryder G., Norman M. D., and Score R. A. 1980. The distinction of pristine from meteorite-contaminated highlands rocks using metal compositions. Proceedings, 11th Lunar and Planetary Science Conference. pp. 471–479.

Salpas P. A., Taylor L. A., and Lindstrom M. M. 1987. Apollo 17 KREEPy basalts—Evidence for nonuniformity of KREEP. *Journal of Geophysical Research* 92:E340–E348. https://doi.org/10.1029/JB092iB04p0E340.

Scholten F., Oberst J., Matz K.-D., Roatsch T., Wählisch M., Speyerer E. J., and Robinson M. S. 2012. GLD100: The near-global lunar 100 m raster DTM from LROC WAC stereo image data. *Journal of Geophysical Research* 117: E00H17. https://doi.org/10.1029/2011je003926.

Sharma P., Kubik P. W., Fehn U., and Gove H. E. 1990. Development of ^{36}Cl standards for AMS. *Nuclear Instruments and Methods in Physics Research* B52:410–415. https://doi.org/10.1016/0168-583X(90)90447-3.

Sharma P., Bourgeois M., Elmore D., Granger D., Lipschutz M. E., Ma X., Miller T., Mueller K., Rickey F., Simms P., and Vogt S. 2000. PRIME lab AMS performance, upgrades and research applications. *Nuclear Instruments and Methods in Physics Research B* 172:112–123. https://doi.org/10.1016/S0168-583X(00)00132-4.

Shirley K. A., Zanetti M., Jolliff B., Van der Bogert C. H., and Hiesinger H. 2016. Origin of discrepancies between crater size-frequency distributions of coeval lunar geologic units via target property contrasts. *Icarus* 273:214–223. https://doi.org/10.1016/j.icarus.2016.03.015.

Shkuratov Y., Kaydash V., and Videen G. 2012. The lunar crater Giordano Bruno as seen with optical roughness imagery. *Icarus* 218:525–533. https://doi.org/10.1016/j.icarus.2011.12.023.

Simonds C. H. 1975. Thermal regimes in impact melts and the petrology of the Apollo 17 Station 6 boulder. Proceedings, 6th Lunar Science Conference. pp. 641–672.

Simonds C. H., Warner J. L., and Phinney W. C. 1973. Petrology of Apollo 16 poikilitic rocks. Proceedings, 4th Lunar Science Conference. pp. 613–632.

Speyerer E. J., Povilaitis R. Z., Robinson M. S., Thomas P. C., and Wagner R. V. 2016. Quantifying crater production and regolith overturn on the Moon with temporal imaging. *Nature* 538:215–220. https://doi.org/10.1038/nature19829.

Spray J. G. and Thompson L. M. 2008. Constraints on central uplift structure from the Manicouagan impact crater. *Meteoritics & Planetary Science* 43:2049–2057. https://doi.org/10.1111/j.1945-5100.2008.tb00660.x.

Spray J. G., Thompson L. M., Biren M. B., and O'Connell-Cooper C. 2010. The Manicouagan impact structure as a terrestrial analogue site for lunar and martian planetary science. *Planetary and Space Science* 58:538–551. https://doi.org/10.1016/j.pss.2009.09.010.

Spudis P. D. and Ryder G. 1981. Apollo 17 impact melts and their relation to the Serenitatis basin. In *Multi-ring basins: Formation and evolution*, edited by Schultz P. H. and Merrill R. B. Proceedings of the Lunar and Planetary Science Conference. New York: Pergamon Press. pp. 133–148.

Spudis P. D. and Sliz M. U. 2017. Impact melt of the lunar Crisium multiring basin. *Geophysical Research Letters* 44:6. https://doi.org/10.1002/2016gl071429.

Spudis P. D., Wilhelms D. E., and Robinson M. S. 2011. The Sculptured Hills of the Taurus Highlands: Implications for the relative age of Serenitatis, basin chronologies and the cratering history of the Moon. *Journal of Geophysical Research* 116:E00H03. https://doi.org/10.1029/2011je003903.

Stöffler D., Knöll H.-D., Marvin U. B., Simonds C. H., and Warren P. H. 1980. Recommended classification and nomenclature of lunar highland rocks—A committee report. In *Conference on the lunar highlands crust*, edited by Papike J. J. and Merrill R. B. Houston, Texas: Pergamon Press. pp. 51–70.

Stöffler D., Ryder G., Ivanov B. A., Artemieva N. A., Cintala M. J., and Grieve R. A. F. 2006. Cratering history and lunar chronology. In *New views of the Moon*, edited by Jolliff B. L., Wieczorek M. A., Shearer C. K., and Neal C. R. Reviews in Mineralogy and Geochemistry, Vol. 60. Washington, D.C.: Mineralogical Society of America. pp. 519–596. https://doi.org/10.2138/rmg.2006.60.05.

Stöffler D., Hamann C., and Metzler K. 2018. Shock metamorphism of planetary silicate rocks and sediments: Proposal for an updated classification system. *Meteoritics & Planetary Science* 53:5–49. https://doi.org/10.1111/maps.12912.

Stopar J. D., Hawke B. R., Robinson M. S., Denevi B. W., Giguere T. A., and Koeber S. D. 2014. Occurrence and mechanisms of impact melt emplacement at small lunar craters. *Icarus* 243:337–357. https://doi.org/10.1016/j.icarus.2014.08.011.

Tagle R. and Berlin J. 2008. A database of chondrite analyses including platinum group elements, Ni Co, Au, and Cr: Implications for the identification of chondritic projectiles. *Meteoritics & Planetary Science* 43:541–559. https://doi.org/10.1111/j.1945-5100.2008.tb00671.x.

Therriault A. M., Fowler A. D., and Grieve R. A. F. 2002. The Sudbury Igneous Complex: A differentiated impact melt sheet. *Economic Geology* 97:1521–1540. https://doi.org/10.2113/gsecongeo.97.7.1521.

Van der Bogert C. H., Hiesinger H., Dundas C. M., Krüger T., McEwen A. S., Zanetti M., and Robinson M. S. 2017. Origin of discrepancies between crater size-frequency distributions of coeval lunar geologic units via target property contrasts. *Icarus* 298:49–63. https://doi.org/10.1016/j.icarus.2016.11.040.

Vaniman D. T. and Papike J. J. 1980. Lunar highlands melt rocks: Chemistry, petrology and silicate mineralogy. In *Conference on the lunar highlands crust*, edited by Papike J. J. and Merrill R. B. New York: Pergamon Press. pp. 271–337.

Wagner R. V. and Robinson M. S. 2014. Distribution, formation mechanisms, and significance of lunar pits. *Icarus* 237:52–60. https://doi.org/10.1016/j.icarus.2014.04.002.

Warren P. H. 1993. A concise compilation of petrologic information on possibly pristine nonmare Moon rocks. *American Mineralogist* 78:360–376.

Warren P. H. 1994. Lunar and Martian meteorite delivery services. *Icarus* 111:338–363. https://doi.org/10.1006/icar.1994.1149.

Warren P. H., Ulff-Møller F., and Kallemeyn G. W. 2005. "New" lunar meteorites: Implications for composition of the global lunar surface, lunar crust, and the bulk Moon. *Meteoritics & Planetary Science* 40:477–506. https://doi.org/10.1111/j.1945-5100.2005.tb00169.x.

Wasson J. T. and Kallemeyn G. W. 1988. Compositions of chondrites. *Philosophical Transactions of the Royal Society of London Series A, Mathematical and Physical Sciences* 325:535–544. https://doi.org/10.1098/rsta.1988.0066.

Wilhelms D. E. 1987. The geologic history of the Moon. U.S. Geological Survey Professional Paper #1348. 329 p.

Williams J.-P., Paige D. A., Plescia J. B., Pathare A. V., and Robinson M. S. 2014. Crater size-frequency distributions on the ejecta of Giordano Bruno (abstract #2882). 45th Lunar and Planetary Science Conference. CD-ROM.

Williams J.-P., Sefton-Nash E., and Paige D. A. 2016. The temperatures of Giordano Bruno crater observed by the Diviner Lunar Radiometer Experiment: Application of an effective field of view model for a point-based data set. *Icarus* 273:205–213. https://doi.org/10.1016/j.icarus.2015.10.034.

Withers P. 2001. Meteor storm evidence against the recent formation of lunar crater Giordano Bruno. *Meteoritics & Planetary Science* 36:525–529.

Wittmann A. and Korotev R. L. 2013. Iron-nickel(-cobalt) metal in lunar rocks revisited (abstract #3035). 44th Lunar and Planetary Science Conference. CD-ROM.

Wittmann A., Korotev R. L., Jolliff B. L., Chennaoui-Aoudjehane H., and Irving A. J. 2014a. Petrology and chemistry of a lunar feldspathic impact melt rock meteorite from Oued Awlitis, Morocco. 77th Annual Meeting of the Meteoritical Society, abstract # 5352.

Wittmann A., Korotev R. L., Jolliff B. L., Lapen T. J., and Irving A. J. 2014b. The petrogenesis of impact basin melt rocks in lunar meteorite Shişr 161. *American Mineralogist* 99:1626–1647. https://doi.org/10.2138/am.2014.4837.

Wittmann A., Korotev R. L., and Jolliff B. L. 2015. Petrogenesis of lunar poikilitic impact melt rock Oued Awlitis 001 (abstract #1141). 46th Lunar and Planetary Science Conference. CD-ROM.

Zanetti M., Hiesinger H., dervan Bogert C. H., Reiss D., and Jolliff B. L. 2011. Aristarchus Crater: Mapping of impact melt and absolute age determination (abstract #2330). 42nd Lunar and Planetary Science Conference. CD-ROM.

Zanetti M., Stadermann A., Jolliff B., Hiesinger H., Van der Bogert C. H., and Plescia J. 2017. Evidence for self-secondary cratering of Copernican-age continuous ejecta deposits on the Moon. *Icarus* 298:64–77. https://doi.org/10.1016/j.icarus.2017.01.030.

Zeigler R. A., Korotev R. L., Jolliff B. L., and Haskin L. A. 2005. Petrography and geochemistry of the LaPaz Icefield basaltic lunar meteorite and source crater pairing with Northwest Africa 032. *Meteoritics & Planetary Science* 40:1073–1101. https://doi.org/10.1111/j.1945-5100.2005.tb00174.x.

Zeng X., Joy K. H., Li S., Pernet-Fisher J., Li X., Martin D. J. P., Li Y., and Wang S. 2018. Multiple lithic clasts in lunar breccia Northwest Africa 7948 and implication for the lithologic components of lunar crust. *Meteoritics & Planetary Science* 53:1030–1050. https://doi.org/10.1111/maps.13049.

SUPPORTING INFORMATION

Additional supporting information may be found in the online version of this article:

Fig. S1. Lunar Reconnaissance Orbiter images of Pierazzo crater.

Table S1. Plagioclase compositions in lunar meteorite Oued Awlitis 001 from electron microprobe analysis.

Table S2. Olivine compositions in lunar meteorite Oued Awlitis 001 from electron microprobe analysis.

Table S3. Pyroxene compositions in lunar meteorite Oued Awlitis 001 from electron microprobe analysis.

Table S4. Troilite and FeNi metal compositions in lunar meteorite Oued Awlitis 001 from electron microprobe analysis.

Table S5. Ilmenite and spinel compositions in lunar meteorite Oued Awlitis 001 from electron microprobe analysis.

Table S6. Whole-rock, fusion crust, and shock melt compositions of lunar meteorite Oued Awlitis 001 from electron microprobe analysis.

Table S7. Young lunar impact craters in best-fit compositional matches to Oued Awlitis 001.